Numerical Study on Hydrodynamics of a Ship Advancing in Confined Waterways

By

HYUNCHUL KIM

Submitted for the Degree of Master of Philosophy

Department of Naval Architecture, Ocean and Marine Engineering

University of Strathclyde

May 2018

Declaration of Authenticity and Author's Rights

This thesis is the result of the author's original research. It has been composed by the author and has not been previously submitted for examination which has led to the award of a degree.

Signed:

Date:

Acknowledgements

I would like to thank Dr. Zhiming Yuan, my supervisor, for his help and encouragement. He provided me guidance in undertaking this work. His enthusiasm also inspired me to carry out the present research. He also provided me the opportunity to use High Performance Computer. Results were obtained by using the EPSRC funded ARCHIE-West High Performance Computer (http://www.archie-west.ac.uk), EPSRC Grant No. EP/K000586/1.

I would also like to thank my Korean supervisor, Professor Sang-Hyun Kim in the Department of Naval Architecture and Ocean Engineering at Inha University for his generous support and guidance.

I would like thank my fellow students for making the days at the research room of department of Naval Architecture, Ocean and Marine Engineering happier and more interesting.

Special thanks to my parents for their eternal love and support.

Glasgow, May 2018

Hyunchul Kim

Abstract

The prediction of ship hydrodynamics in the confined waterways is challenging. It may involve both ship-bottom and ship-bank interactions. When a ship is advancing in shallow water, the hydrodynamic behaviours may vary significantly due to the hydrodynamic interaction between the bottom of the ship hull and the seabed, or so called shallow water effects. The flow velocity in the gap between the ship bottom and the seabed increases, which will lead to an increase in ship's sinkage, trim and resistance. Also, the asymmetric flow around a ship induced by the vicinity of banks causes pressure differences between port and starboard sides, which is known as the bank effects. Therefore, an accurate prediction of shallow water and bank effects is essential to minimize the risk of the collision and the grounding for the ships. Flanders Hydraulics Research (FHR) in cooperation with the Maritime Technology Division of Ghent University has carried out shallow model tests in a towing tank equipped with surface-piercing banks and a vertical quay wall with a 1/75 scale model of the KRISO Very Large Crude carrier (KVLCC2). The forces and moments on the KVLCC2 model were obtained at various water depths, lateral distances to the banks. Additionally, the wave elevation was measured between the quay wall and the ship model. The main objective of the present paper is to simulate the complex flow around the ship and predict the hydrodynamic behaviours of a ship when advancing in the confined waterways. To simulate ship hydrodynamics in confined waterways, the CFD programme should be used to get a reliable result. In the present study, a widely used CFD programme, Star-CCM+, will be used to simulate the complex flow phenomena induced by a ship advancing in confined waterways. To evaluate the capability of the CFD software, the numerical data will be compared with the experimental data conducted by FHR. The free surface effect will be taken into account. The results will include the forces and moments acting on the ship, as well as the wave elevation between the quay wall and the ship model. The parametric study will be conducted to investigate the effects of the ship speed, the water depths and the positions in a channel. Discussions will be highlighted on the ship-bank interaction when the water depth Froude number approaches critical value.

Key words: ship hydrodynamics, confined waterways, bank effect, shallow water, KVLCC2, CFD

Contents

List of Tables

List of Figures

Nomenclature

$\overline{u_i}$	Mean flow velocity
$\mathbf{I_{xx}}$	Ship mass moment of inertia in x axis
$\mathbf{I_{yy}}$	Ship mass moment of inertia in y axis
$\mathbf{I_{zz}}$	Ship mass moment of inertia in z axis
$\mathbf{L_{pp}}$	Length between the perpendiculars
$\mathbf{u_i'}$	Turbulent fluctuating velocity
$\mathbf{u_t}$	Fiction velocity
$\mathbf{y^+}$	Dimensionless wall distance
$\boldsymbol{\sigma_{ij}}$	Stress
$\boldsymbol{\tau_w}$	Wall shear stress
2D	Two dimensional
3D	Three dimensional
B	Beam of ship
CFD	Computational Fluid Dynamics
CFL	Courant number
CoG	Centre of gravity
$\boldsymbol{d}$	Distance between the ship and vertical wall
DFBI	Dynamic Fluid Body Interaction
DNS	Direct Numerical Solution
EFD	Experimental Fluid Dynamics
EMSA	European Maritime Safety Agency
FHR	Flanders Hydraulics Research
$\mathbf{F_n}$	Froude number
$\boldsymbol{g}$	Gravitational acceleration
$\boldsymbol{h}$	Water depth
ITTC	International Towing Tank Conference
KVLCC2	KRISO Very Large Crude Carrier 2
LES	Large Eddy Simulation
MAIB	Marine Accident Investigation Branch
RANS	Reynolds-Averaged Navier-Stokes
RPM	Revolution per minute

RSM	Reynolds Stress Model
T	Design draft
TEU	Twenty feet Equivalent Unit
U	Mesh flow speed
UKC	Under-keel clearance
VLCC	Very Large Crude Carrier
VOF	Volume of Fluid
W	Width of tank
$\boldsymbol{k}$	Turbulent kinetic energy
$\boldsymbol{\Delta t}$	Time step
$\boldsymbol{\Delta x}$	Mesh dimension
$\boldsymbol{\varepsilon}$	Dissipation rate
$\boldsymbol{\nu}$	Kinematic viscosity
$\boldsymbol{\rho}$	Density
$\boldsymbol{v}$	Ship speed

1 Introduction

1.1 Background

Recently, the main dimension of ship sizes and the number of large ships have increased dramatically. Moreover, the world trade continues to grow, but at a slow rate in recent year, and the sea transportation plays an important role in this matter as the cheapest and most efficient means of transport over long distances. At the end of 2016, there were around 58,000 vessels in the world trading fleet, with a total deadweight tonnage of 1,778 million. By dead weight tonnage, the world fleet has doubled since 2004 though the rate of growth has slowed in recent years, with a 3 percent increase in 2016. These factors result in an increasing of more vessels sailing in more restricted waters.

The Marine Accident Investigation Branch (MAIB) reports the marine accidents every year. In their reports most accidents were recorded in restricted waters such as coastal waters, port, harbour and canal. According to European Maritime Safety Agency (EMSA), casualty events with a ship due to contact, collision and grounding represent 50% of all casualties with ships in the territorial sea and internal waters of EU States.

When a ship is advancing in confined waterways, the hydrodynamic behaviour varies a lot. In particular, the flow velocity between a ship hull and the bottom of the sea increases and it has a different vertical position in shallow water, which is known as “squat”. The resistance, therefore, gets larger in shallow water than that in deeper water for the same vessel at the same forward speed, which leads to a decrease of manoeuvrability. The course stability of a ship sometimes improves in shallow water. But generally the manoeuvrability gets worse as the water depth decreases. Furthermore, with the presence of a vertical bank, the ship hydrodynamics becomes more complicated. The asymmetric flow around a ship induced by the vicinity of banks causes pressure differences in the port and starboard sides, which is known as the bank effects. So, to predict accurately the squat of a ship is essential at a wide range of speed and water depth, in order to minimize the risk of collisions and the grounding.

1.2 Objective

The overall objective of this study is to simulate the complex flow around the ship and predict the ship hydrodynamics when advancing in the confined waterways using the commercial CFD software (STAR-CCM+). The specific objectives are as follows:

1. To develop a CFD model that can be used to predict the ship hydrodynamics in confined waterways, including the forces and moments on the ship, the sinkage and trim angle of the ship, wave elevation and pressure distribution and to validate the numerical results with experimental data in order to estimate the reliability of the numerical models.
2. To investigate the hydrodynamic forces and moments of a ship advancing at different forward speed in confined waterways.

1.3 Outline of the thesis

The present thesis consists of seven main chapters, each of which covers the following content

Chapter 1 introduces an overview of the problem followed by the background regarding the manoeuvres in confined waterways and details the research aim and objectives that will encourage the readers to have a clear idea of the research scope and targets.

Chapter 2 introduces the basic definitions and concepts of bank effects and ship squat and deals with an in-depth literature review of the present state of ship-bank interaction and ship-bottom interaction in experimental and theoretical or numerical way.

Chapter 3 provides an overall description of the theory of computational fluid dynamics to be used in this study.

Chapter 4 provides the numerical set up for the simulations using the STAR-CCM+ software.

Chapter 5 contains the results of the verification study and also presents the results of the numerical simulation, including forces and moments, sinkage and trim, wave elevation and pressure distribution.

Chapter 6 contains the overall conclusions and a summary given with discussion of the results and remarks on further work.

2 Literature review

2.1 Remarks

This chapter reviews the basic hydrodynamic theory by considering the bank effects and ship squat. The review will follow two ways: theoretical/numerical and experimental methods.

2.2 Main principle

2.2.1 Bank effects

When a ship is advancing along a bank or wall, the well-known phenomenon occurs, so called bank effects. In this case, a lateral force and a yawing moment are generated, which will push the ship towards the bank and to pull the bow away from the bank causing the vessel swing. (Kobylinski, 2014) If a rudder action is taken towards the bank, it will counteract the swing and the waterway will be safe. This phenomenon may be explained in a simple way. When the ship is advancing close to a wall, the speed of the flow between the hull and the bank will increase due to the reduction of the cross section area between the bank and the ship. But the ship hull is far away from the other side of the bank. Therefore, the flow speed on the other side of the ship does not change comparing to the open water case. According to the Bernoulli's law, if the water velocity increases, in consequence the pressure will be reduced. The difference of pressure distributed on ship's two sides will induce the suction force, which is directed from the higher pressure side towards the lower pressure side. This suction force will attract the ship closer to the bank. On the other hand, the bow of the ship is rejected from the bank because the pressure around the bow increases, which is called a bow cushion when the ship is advancing proximity of the wall. As a result, a yawing moment is pushing the bow of the ship away from the wall, as shown in Figure 2-1.

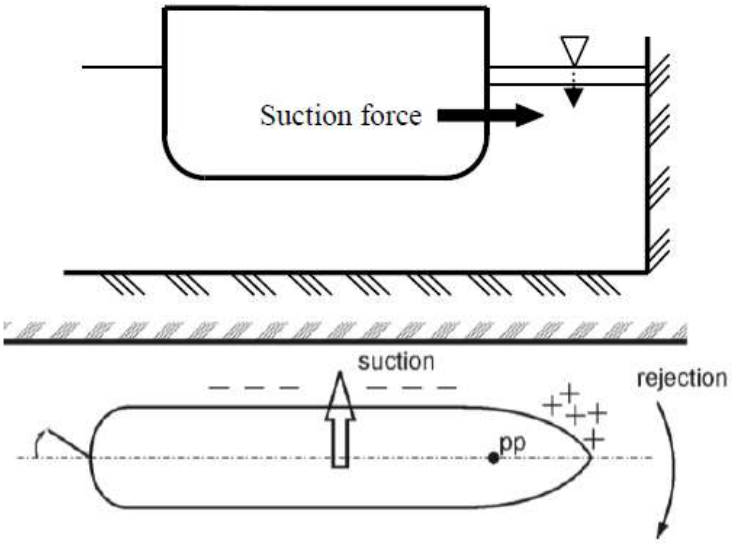

Figure 2-1 Effect of proximity of the bank **(Kobylinski, 2014)**

2.2.2 Ship squat

Squat occurs both in deep and confined water. When a ship is advancing in the shallow water, a pressure drop along the hull of the ship occurs, according to the Bernoulli principle. Consequently, the pressure distributed in the bow and aft parts of the ship will increases. But the pressure distributed in the bottom of the midship part decreases. Generally, the pressure will not drop equally in the fore and aft parts of the ship. As a result, the pitch moment will cause the ship to trim. The magnitude of squat depends on the hull shape, the side and under keel clearance (UKC) and the sailing speed.

As shown in Figure 2-2, when the under keel clearance of ship B is smaller, the flow is compressed to pass a small gap with increased speed. According to Bernoulli's law, if the flow speed under the ship increases, the pressure under the ship drops. This phenomenon results in the decrease of the pressure distributed over the ship's bottom. A vertical force pointing downwards will cause the ship to sink. This combination of sinkage and trim is referred to as squat.

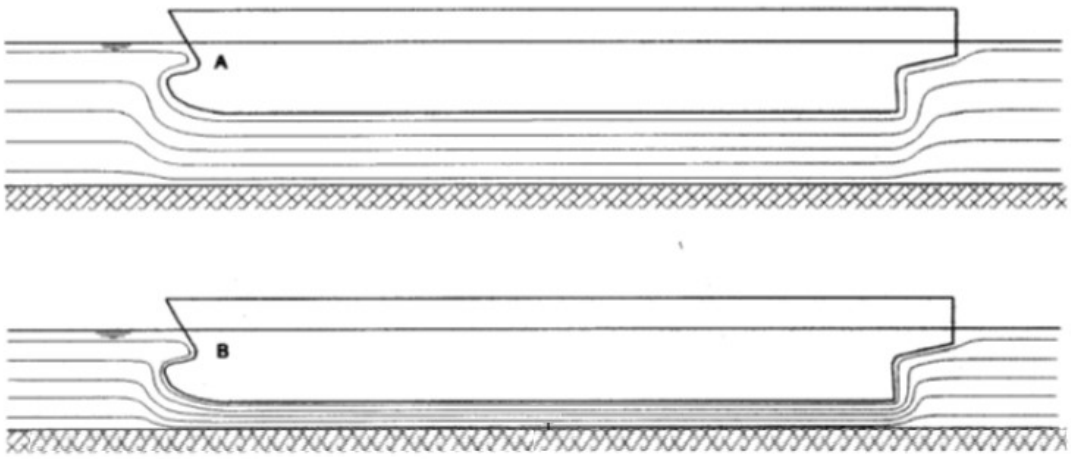

Figure 2-2 The effect of shallow water (*Source : Norwest Interaction, Hydrodynamic training programme*)

2.3 Historical summary

2.3.1 Theoretical and numerical methods

Tuck (1966) used the slender body theory to obtain sinkage and trim of a ship in shallow waters at both sub-critical and super-critical speeds. The simple calculation formulas were derived for sinkage and trim. Tuck's theoretical method based on the slender body theory has been widely used for predicting the squat of the ship in shallow water. Beck, et al. (1975) solved the boundary value problem to predict the sinkage, trim and resistance of the ship advancing in a dredged channel for different depth Froude numbers. The dredged channel geometry that was used in the study was surrounded by shallow water regions, with the vertical wall on the side of the channel. It was concluded that the exterior shallow regions had a considerable effect on the sinkage, trim and resistance in restricted channels. Newman (1969) used the potential flow theory to calculate the interaction between a ship and a vertical wall. Beck (1977) applied this theory to point out the investigation of the under keel clearance on bank effects. The results were compared with model tests from Norrbin (1974) on a ship advancing at different lateral positions and water depth between two vertical walls.

Gates and Herbich (1977) evaluated the limitation of dimensions of existing channels based on increasing ship sizes. Yasukawa (1991) used a hybrid model of the potential theory, the slender body and panel method to investigate the manoeuvrability of the ship in and an arbitrary shaped canal. Miao (2003) used the potential flow method to calculate the sway force and yaw moment in a rectangular channel, as well as the wave pattern at the free surface and the pressure distribution were calculated based upon the same theoretical method. The numerical results were compared to the model tests measurements carried out at the Australian Maritime College. The reasonable hydrodynamics in deep water ($h/T > 1.5$) was satisfying but in shallow water it was not good. Gourlay (2008) studied one-dimensional slender body theories to predict the squat of a ship advancing in shallow water. The general Fourier method was presented to calculate the squat of the ship advancing in arbitrary channel, the rectangular canal and the dredged channel. Alderf et al. (2009) used the finite element method for numerically modelling dynamic squat. This study resulted in the dynamic responses of the ship in highly restricted canals on irregular shaped bottom. Kumar and Anantha Subramanian (2007) investigated the influence of the walls in drag estimation based upon the numerical calculations and model tests with two barge models of different scales by using a volume of fluid (VOF) model. The results represented that the influence of the walls could be negligible if the tank width was larger than 5 times of the beam of the ship.

As computer technique has developed rapidly, the numerical prediction of the hydrodynamics using Computational Fluid Dynamics (CFD) techniques has become possible. CFD method is capable of prediction of ship manoeuvrability in viscous flow, considering the free surface and nonlinear effects. Jachowski (2008) studied the squat of a ship in shallow water using RANS solver. The KRISO container ship was used as model ship for the calculation of the squat for different water depths at various ship speeds. The results were compared with the results calculated by using the empirical formulae. Wang, et al. (2010) calculated the viscous hydrodynamic forces on the hull of a ship at different lateral positions and water depths in a channel using Reynolds-Averaged Navier-Stokes equation (RANS) method. The results of calculations were compared with the results from the model tests (Vantorre, 2002). Chetvertakov, et al. (2011) created a regression model for bank effect through numerical calculations. The

model took the drift angle into account and was compared with model tests. The panel method (3D first order Rankine) is adopted to calculate the sway force and yaw moment induced by a vertical bank and a sloped (1/3) bank on an 8000 TEU container carrier. These calculations were compared with the published open data on bank effects (Lataire, et al., 2009). Zou, et al. (2011), Zou and Larsson (2013) investigated the bank effects and reported an extensive comparison between CFD calculations and model tests with a VLCC at various water depths at low speed along different surface-piercing banks. Their study also represented verification and validation based on the grid convergence study and the exploration of modelling error in RANS calculation to investigate more precise and reliable predictions of the bank-effects. Zou and Larsson (2013) especially considered the effect of propeller RPM using CFD. Hoydonck, et al. (2015) simulated ship-bank and ship-bottom interaction by two different CFD software. The author compared the CFD results with other results based on potential theory. However, the results of the potential code computation were quite incorrect compared to EFD results.

2.3.2 Experimental methods

Fuehrer (1978) carried out model tests with a tanker model in a canal with sloped banks and stepped banks at different lateral positions to describe the influence of lateral forces on the asymmetrical ship, the geometry of the bank, the heading and the forward speed. Römisch (1978) analysed the same model tests to obtain the proper width of a canal for a safe navigation and proposed a design guideline for the minimal width of the canal. Fuehrer and Römisch (1983) carried out a comprehensive set of model tests to describe the relation between the external forces induced by bank effects and the rudder force and developed the empirical equation for predicting rudder force. Dand (1982) performed extensive tank test regarding ship-bank interaction and some preliminary behaviour of the influence parameters stated on previous. These ship models were towed along surface-piercing banks as well as semi-submerged banks. The tests were carried out in a classic towing tank as well as a circulation water channel. The results of the longitudinal force, lateral force, yaw moment and vertical sinkage

and trim are discussed. Norrbin (1985) conducted extensive analytical and experimental studies on the bank effects in details. These tests are based on model tests with the propelled tanker model and the researchers presented empirical formulas for various bank configuration including vertical, sloped and submerged banks at different forward speeds. Ch'ng, et al. (1993) improved Norrbin's research and carried out a series of model tests and developed an empirical formula to evaluate forces acting on hull by the bank. Li, et al. (2001) continued Norrbin's study and carried out model tests on bank effects in extreme shallow water and near bank conditions for three different hull forms (a tanker, a ferry and a catamaran). The influence of the ship speed, water depth, bank distance, bank inclination, propeller action, bank submergence was evaluated. Vantorre, et al. (2003) investigated the influence of the water depth, ship-to-bank distance, ship speed and propeller on the hydrodynamic forces and moments based on a systematic captive model tests conducted at Flanders Hydraulics Research (FHR), Belgium, for three ship models advancing in a tank with the vertical surface-piercing bank. Empirical formulae for the calculation of ship-bank interaction forces were proposed. Gronarz (2009) carried out model tests for an inland waterway ship towed under a drift angle. The coupling terms of the combination between the bank effects and the drift angles were explained. A mathematical regression model was proposed to improve the consideration of bank effects. Hoydonck, et al. (2015) carried out the model tests in their towing tank equipped with surface-piercing banks and a vertical wall. the empirical results were compared with two different CFD results and the results of potential flow computations to investigate the benefits of each method.

3 Computational methods

3.1 Remarks

The key topics covered in this chapter include: the governing equations for Computational Fluid Dynamics (CFD) modelling, description of the turbulence models, discretization schemes and near wall modelling. The following is based on the book of Peric and Joel (1997) which gives a good introduction to computational fluid dynamics.

3.2 Governing equations

Computational Fluid Dynamics (CFD) is based on three fundamental governing equations, which is the Continuity equation, Navier-Stokes equation. The continuity equation is a mass conservation equation given by Peric and Joel (1997).

$$\frac{\partial \rho}{\partial t} + \frac{\partial (\rho u_i)}{\partial x_i} = 0 \tag{3.1}$$

where ρ is the density of the fluid, t is time, x_i are spatial coordinates and u_i is the velocity field components along the spatial coordinate directions.

The first and second terms describe the rate of change of density with time and the gradient of mass change along the three spatial coordinate directions respectively. This equation is the differential form of the continuity equation. In this study, fluid is considered to be incompressible. For incompressible fluids with no source, equation (3.1) simplifies to

$$\frac{\partial u_i}{\partial x_i} = 0 \tag{3.2}$$

The Navier-Stokes equation is a momentum conservation equation given in equation (3.3). The equation is derived by setting the rate of change of the momentum in a particular component direction equal to the net force acting on the element in that direction (due to the surface stress) plus the gravitational and external forces.

$$\frac{\partial(\rho u_i)}{\partial t} + \frac{\partial(\rho u_j u_i)}{\partial x_j} = \frac{\partial \sigma_{ij}}{\partial x_j} + \rho g_i \tag{3.3}$$

where g_i is the gravitational acceleration and σ_{ij} is the stress on the fluid, which is expressed as

$$\sigma_{ij} = -p\delta_{ij} + \mu\left(\frac{\partial u_i}{\partial x_j} + \frac{\partial u_j}{\partial x_i}\right) \tag{3.4}$$

The momentum conservation equation (3.3) consists of four terms; the transient term, the convective term, the diffusive term and the source term. Those equations represent five equations; three Navier-Stokes equations, one for each spatial direction, one continuity equation and one energy equation. For laminar flow problems, five unknowns are represented: the three velocity components and the pressure and the temperature.

The governing equations are formed by the mass and momentum conservation equations, which are solved simultaneously to describe fluid flow. It is the most correct numerical way to solve the Navier-Stokes equations for solving turbulent flows, that is known as the Direct Numerical Solution (DNS) method. However, it is extremely difficult to use the DNS method for practical computation, since it often is too time consuming, that is not appropriate for practical applications. Therefore, the DNS method is suitable only for fluid flows at low Reynolds number with simple flow geometries.

Instead of the DNS method, the RANS equation which is the time averaged equations is used for modelling turbulent flow in practical CFD application. The main assumption in this approach is to decompose the transient velocity into a mean flow velocity, $\overline{u_i}$ and turbulent fluctuating velocity parts, u_i' and solve the resulting simplified equations.

$$u_i = \overline{u_i} + u_i' \tag{3.5}$$

Where the averaging is a short time averaging, equalizing turbulent fluctuations.

Inserting this expression for the velocities into the Navier-Stokes equation, and averaging all terms in the equation in order to describe the mean behaviour the Reynolds Averaged Navier-Stokes Equation (RANS) arises:

$$\rho\left(\frac{\partial \overline{u_i}}{\partial t} + \overline{u_i}\frac{\partial \overline{u_i}}{\partial x_j}\right) = \rho\overline{g_i} + \frac{\partial}{\partial x_j}\left(\overline{\sigma_{ij}} - \rho\overline{u_i' u_j'}\right) \tag{3.6}$$

comparing this with the Navier-Stokes equation, (3.2), it is observed that an extra term occurs. This term is the Reynolds stress tensor, given by:

$$-\rho\overline{u_i' u_j'} = \begin{bmatrix} -\rho\overline{u_1' u_1'} & -\rho\overline{u_1' u_2'} & -\rho\overline{u_1' u_3'} \\ -\rho\overline{u_2' u_1'} & -\rho\overline{u_2' u_2'} & -\rho\overline{u_2' u_3'} \\ -\rho\overline{u_3' u_1'} & -\rho\overline{u_3' u_2'} & -\rho\overline{u_3' u_3'} \end{bmatrix} \tag{3.7}$$

Where the subscripts 1, 2, and 3 denote the three axial directions.

As $-\rho\overline{u_1' u_2'}$ is equal to $-\rho\overline{u_2' u_1'}$ etc., the Reynolds stress tensor consists of six independent stresses. This means that including turbulent fluctuations the system consists of 5+6=11 independent variables and still only 5 equations. This is referred to as the closure problem turbulence.

A huge number of approaches have through the last decades been developed to close the problem of turbulence. Some theories are more accepted and tested than others, but in general the quality of the different theories is application dependent.

3.3 Turbulence models

The RANS equations is obtained to model the turbulent flow. The Navier-Stokes equations are decomposed into a mean flow velocity and a fluctuating velocity components. This results in the equations for the mean quantities which are the same as the original equations, except the extra Reynolds stress tensor parts, given by equation (3.7).

The challenge is to present closure of the governing equations for modelling the

Reynolds stress tensor with regard to the mean flow quantities. The most usual method to deal with turbulence is to use turbulence models in which the turbulent features of the flow are not resolved in time. Turbulence models are used to evaluate turbulent viscosity. There are several methods available for turbulence modelling:

(1) Linear eddy viscosity models: one-equation models and two-equation models

(2) Nonlinear eddy viscosity models

(3) Reynolds Stress Model (RSM)

(4) Large Eddy Simulation (LES)

The most commonly used approach in engineering practice nowadays is to solve the Reynolds Averaged Navier-Stokes equations coupled with a turbulence model.

The linear eddy viscosity models, mainly the two-equation model, are the most common type of turbulence models used for practical engineering applications (Wilcox, 2006). The following section provides a brief description of the two-equation models, particularly $k-\varepsilon$ models which is used in this study. That is because the models has been widely used in similar studies (Tezdogan, et al., 2016), (Quérard, et al., 2008).

For the $k-\varepsilon$ turbulence model, the turbulent viscosity is connected with turbulent kinetic energy (k) and dissipation rate (ε).

To close the set of equations we have to introduce a turbulence model. To see what a reasonable model might be, we note that in laminar flows, the energy dissipation and transport of mass, momentum and energy normal to the streamlines are mediated by the viscosity, so it is natural to assume that the effect of turbulence can be represented as an increased viscosity. This leads to the eddy-viscosity model for the Reynolds stress:

$$-\rho\overline{u_i'u_j'} = \mu_t\left(\frac{\partial\overline{u}_i}{\partial x_j}+\frac{\partial\overline{u}_j}{\partial x_i}\right)-\frac{2}{3}\rho\delta_{ij}k \tag{3.8}$$

And the eddy-diffusion model for a scalar:

$$-\rho\overline{u_j'\phi'} = \Gamma_t\frac{\partial\bar{\phi}}{\partial x_j} \tag{3.9}$$

In equation (3.8), *k* is the turbulent kinetic energy:

$$k = \frac{1}{2}\overline{u_i' u_i'} = \frac{1}{2}\left(\overline{u_x' u_x'} + \overline{u_y' u_y'} + \overline{u_z' u_z'}\right) \tag{3.10}$$

The transport equations for *k* is derived in the book of Wilcox (2006) and continue as follows:

$$\frac{\partial(\rho\epsilon)}{\partial t} + \frac{\partial(\rho u_j \epsilon)}{\partial x_j} = \mathrm{C}_{\epsilon 1} P_k \frac{\epsilon}{k} - \rho C_{\epsilon 2} \frac{\epsilon^2}{k} + \frac{\partial}{\partial x_j}\left(\frac{\mu_t}{\sigma_\epsilon}\frac{\partial \epsilon}{\partial x_j}\right) \tag{3.11}$$

In this model, the eddy viscosity is expressed as:

$$\mu_\mathrm{t} = \rho C_\mu \frac{k^2}{\epsilon} \tag{3.12}$$

This $k-\varepsilon$ model is based on equations (3.11) and (3.12) and contains five parameters; the most commonly used values for them are:

$$\mathrm{C}_\mu = 0.09, \qquad C_{\epsilon 1} = 1.44, \qquad C_{\epsilon 2} = 1.92, \qquad \sigma_k = 1.0, \qquad \sigma_\epsilon = 1.3 \tag{3.13}$$

3.4 Discretization scheme

CFD provides many different discretization schemes for temporal and spatial parts of the governing equations, some of which are only available in conjunction with specific models.

There are first and second order schemes available in the steady and unsteady problems for temporal discretization. For a limited subset of flow modelling scheme, such as the laminar coupled energy model, only explicit temporal schemes are available. For spatial discretization, the first and second order upwind schemes can be used, with additional options such as bounded central differencing schemes and central differencing schemes, which are limited particular models, such as large eddy simulation (LES).

In this study, the first order unsteady implicit scheme is selected for temporal discretization. The discretisation as first order offers a good compromise between accuracy and time required to run the simulation (Tezdogan, et al., 2016). Implicit time integration means that the flow variables are evaluated at the future time, $\mathrm{t} + \Delta\mathrm{t}$. Since these are not known in the current time step, the implicit time integration requires the

iterations. In comparison to the explicit time integration, where the flow variables are evaluated at the current time so that iteration is avoided, the implicit time integration is more computationally expensive. On the other hand, the implicit time integration is unconditionally stable, meaning that it is stable for all time step sizes (Versteeg & Malalasekera, 2007).

For the spatial discretization, the second order upwind scheme will be selected in this study. The benefits of the second order schemes for spatial discretization are well noted and the lower order option is not investigated in this work; the increased demands of the second order scheme are expected to be well worth any additional computational demands.

When starting a numerical calculation process, the lower order schemes, such as the first order upwind scheme are usually recommended, as these are more stable. However, a high degree of unphysical diffusion in the solution can be obtained due to the low accuracy (Demuren, 1985), which is known as numerical diffusion. If the flow field becomes stable, a higher order scheme should therefore be used to obtain a more physically precise result. The second order upwind scheme is often regarded as a suitable discretization scheme because it provides a good balance between the numerical accuracy and stability (ITTC, 2011).

3.5 Law of the wall

The law of the wall is explained that the average velocity of a turbulent flow at some point is proportional to the logarithm of the distance from that point to the wall. The y^+ value is the dimensionless distance from the wall, which is given by:

$$y^+ = \frac{y u_\tau}{\nu} \tag{3.14}$$

where ν is the kinematic viscosity and u_τ is the friction velocity, which is given by,

$$u_\tau = \sqrt{\frac{\tau_\omega}{\rho}} \tag{3.15}$$

where τ_ω is the wall shear stress and ρ is the fluid density (White, 2006).

When numerically setting up the simulation, controlling the y^+ value plays an important role. One should set up the numerical simulation properly based on which wall treatment is selected. There are the sets of near wall modelling assumption for each turbulence model in wall treatment of STAR-CCM+. This term avoids confusion with the term wall function, which typically refers to only one type of wall treatment. As shown in Figure 3-1, STAR-CCM+ provides three types of wall treatment models, depending on the turbulence model.

The low y^+ wall treatment is suitable only for low Reynolds number turbulence models in which it is assumed that the viscous sublayer is properly resolved and is therefore solving the boundary layer (equation 3.16), which means no wall laws are required. For this model, it is important to try to keep y+ values in between 1 to 5.

$$u^+ = y^+ \tag{3.16}$$

The high y^+ wall treatment means the wall function type approach, where it is assumed that the near wall cell falls within the logarithmic region of the boundary layer (equation 3.17).

$$u^+ = \frac{1}{k(von\ Karman's\ (const. \cong 0.41))} \ln(y^+) + B(\text{const.} \cong 5.1) \tag{3.17}$$

The all y^+ wall treatment is a hybrid treatment model that attempts to model similarly and the low y^+ wall treatment for finer meshes and the high y^+ wall treatment for coarser meshes. It also deals with the desirable characteristic of producing reasonable answers for intermediate meshes resolution, which is done, in other words, when the wall cell centroid is within the buffer region of the boundary layer. All y^+ wall treatment is automatically selected when the $k-\varepsilon$ turbulence model is selected

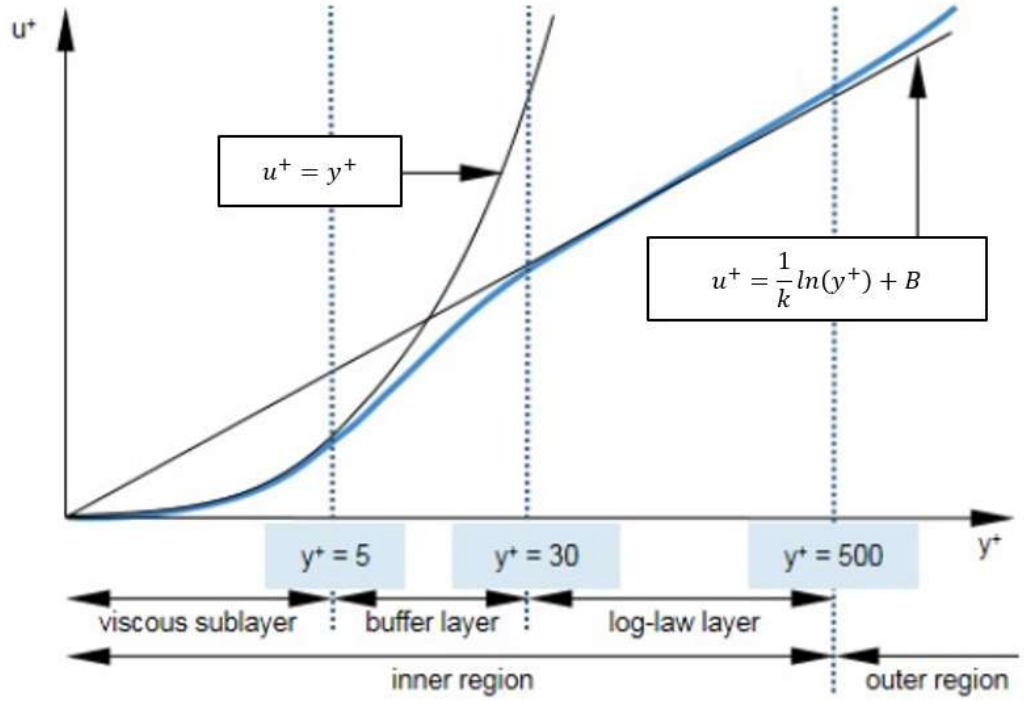

Figure 3-1 $\mathbf{y^+}$ value regions

4 Simulation set up

4.1 Remarks

In the previous chapters, the computational methods were described to define the appropriate conditions and numerical method to be applied in the governing equations used in the present work. This chapter will describe the simulation set-up for numerical calculations based on recommendations from CD-Adapco (2017), including the computational domain definition, mesh generation, boundary condition, physics models. In the present study, the most widely used CFD programme Star-CCM+ will be used to simulate the complex flow phenomena when a ship is advancing in confined waterways. Different parameters that have influence on the calculation of the interaction forces and moments are specified. The characteristics of the ships model will also be introduced. The establishment of the configuration of the mesh and the computational criteria and boundary conditions are described in details in this chapter.

4.2 Geometry

4.2.1 Ship

The ship model used in this study is a 1/75 model scale of the KRISO Very Large Crude Oil Carrier (KVLCC2). For this hull form, the model tests were carried in the shallow water towing tank at Flanders Hydraulics Research (FHR), in cooperation with the Maritime Technology Division of Ghent University, Belgium (Hoydonck, et al., 2015) which is equipped with surface-piercing banks and a vertical quay wall. KVLCC2 is a standard ship model used for ship hydrodynamics research, and it is widely used in ITTC research programme. The geometry of the model is available at the website of SIMMAN2014. The main particulars of KVLCC2 in model scale used for computational test are given in Table 4-1, and the 3D longitudinal view of the ship model is shown in Figure 4-1.

Table 4-1 Main particulars of KVLCC2 (model scale)

Parameter	Unit	1/75 model scale
Length (L_{pp})	m	4.2667
Draft Amidships (T_m)	m	0.2776
Vertical CoG (KG)	m	0.2776
Longitudinal CoG (X_G)	m	0.1449
Displacement (∇)	m^3	0.7410
Block coefficient (C_B)	-	0.8098
Mass (m)	kg	736.2
Moment of inertia about x axis (I_{xx})	$kg{\cdot}m^2$	41.0
Moment of inertia about y axis (I_{yy})	$kg{\cdot}m^2$	797.3
Moment of inertia about z axis (I_{zz})	$kg{\cdot}m^2$	831.5

Figure 4-1 3D longitudinal view of the KVLCC2 model in Star-CCM+

4.2.2 Computational domain

The towing tank used in this study is equipped with a surface-piercing bank and a vertical quay wall along the full length of the tank (Hoydonck, et al., 2015). The lateral cross section of the computational domain and the coordinate system used in this study is the same as the geometry shown in Figure 4-2, where the d is the ship-to-bank distance, h is the water depth and $\tan\theta = 1/4$. As shown in the Figure, the coordinate system is defined as a body-fixed and right-handed Cartesian system, with the origin located at intersection of the undisturbed free surface and midship of the body. The

axes *x, y, z* are set to direct towards the bow, to starboard and downwards, respectively.

ITTC (2017) recommends that in resistance, sinkage and trim simulations, the inlet boundary should be placed at least $1L_{pp}$ in front of the ship, whereas their outlet should be located at least $2L_{pp}$ behind the ship to avoid any wave reflection from the boundary walls. Therefore the inlet boundary was positioned $1.5L_{pp}$ in front of the ship, and the outlet boundary $2.5L_{pp}$ behind the ship. The top of the domain is placed $0.5L_{pp}$ above the waterline in this study. The overview of the computational domain is shown in Figure 4-3.

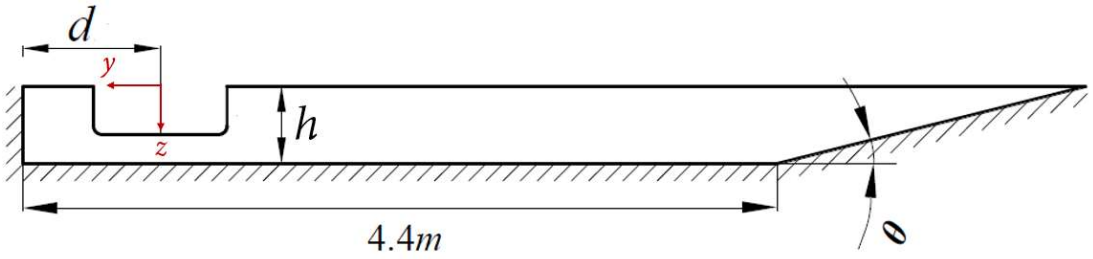

Figure 4-2 Cross section of the tank geometry with the coordinate system

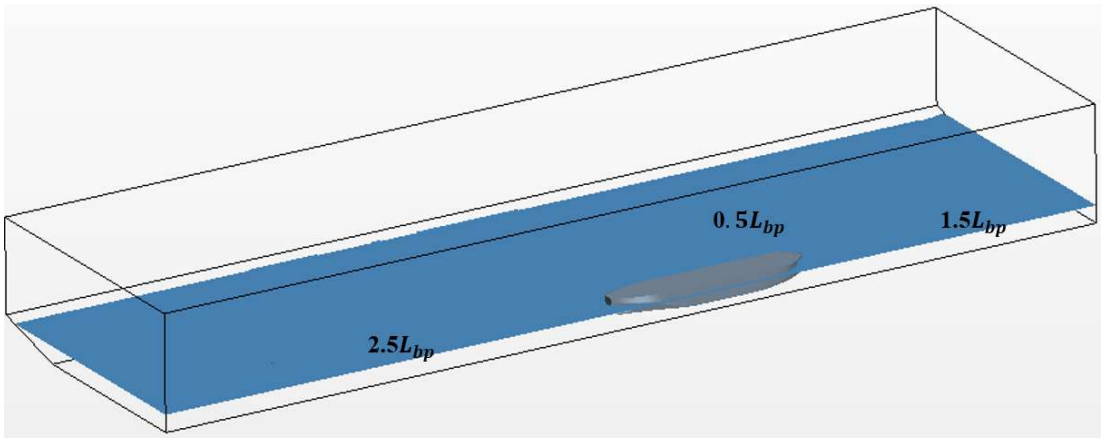

Figure 4-3 Overview of the computational domain

4.3 Boundary condition

The setting of the boundary conditions and initial conditions of the CFD model depends on the physics of the problem to be solved. The proper selection of the boundary condition plays an important role to obtain accurate solution and prevent unnecessary computational cost in CFD calculations (Date & Turnock, 1999). A general view of the computational domain with the KVLCC2 hull model and the definition of boundary conditions are shown in Figure 4-4.

A velocity inlet boundary condition is set in the boundary far in front of the ship, where the flat waves are created. The pressure outlet boundary condition is set in the boundary far behind the ship, which will prevent the backflow. It could also fix undisturbed hydrostatic pressure at the boundary. On the top of the domain, a velocity inlet boundary condition is set, where the boundary pressure is extrapolated by using reconstruction gradients. The bottom and the surface-piercing tank walls are modelled as no-slip walls, which have the relative velocity with reference to the ship. The pressure resistance fluctuation is usually generated because of the reflected waves from the non-physical side boundaries. Therefore, the VOF damping method of the software package with a damping length of 5 m ($1.172\mathrm{L_{pp}}$) which is referred to similar study (Tezdogan, et al., 2016) is applied on the inlet and outlet boundaries to avoid the wave reflection in all the cases.

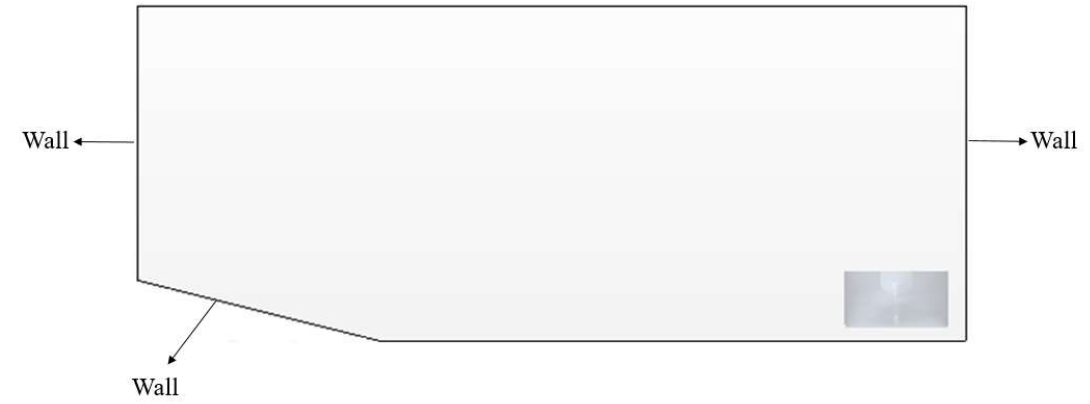

(a)

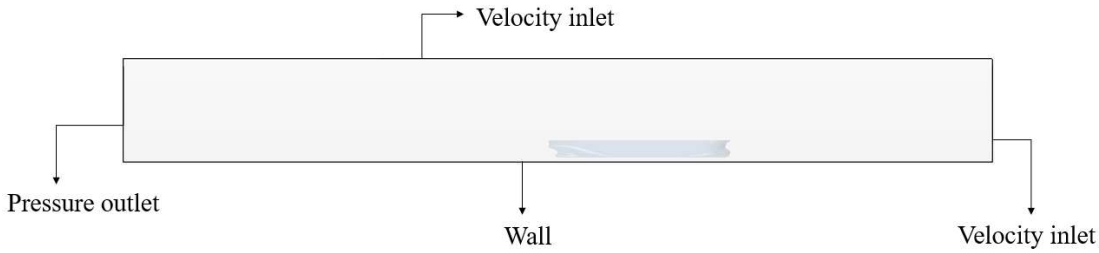

(b)

Figure 4-4 The computational domain and the applied boundary conditions. (a) Cross section at x=0; (b) longitudinal section at y=0

4.4 Simulation cases

Table 4-2 lists the test matrix of the cases without propulsion. Cases 1 – 3 have the same water depth (h/T), while the distance between the ship and the vertical wall (d/B) is different. Therefore, this set of test cases is used to represent ship-bank interaction. Cases 3 – 5 have the same d/B, while h/T is different. Therefore, this set of test cases is used to represent the ship-bottom interaction. In Cases 1 –5, the Froude number F_n is 0.055 (v = 0.356 m/s). Table 4-3 lists the test condition of ship speeds at the specific distance to the bank and water depth of Case 1.

Table 4-2 Matrix of test conditions for validation study

	d/B	h/T	F_n
Case 1	0.67	1.35	0.055
Case 2	0.76	1.35	0.055
Case 3	1.26	1.35	0.055
Case 4	1.26	1.5	0.055
Case 5	1.26	1.1	0.055

Table 4-3 Test condition of ship speeds for Case 1

	F_n
Case 1	0.025, 0.05, 0.075, 0.1, 0.125, 0.15

4.5 Mesh generation

In order to refine the mesh density, the volumetric controls are used with specified volume shapes. Star-CCM+ has three different volumetric mesh topologies: Polyhedral Mesher, Tetrahedral Mesher and Trimmed Cell Mesher. The trimmed cell mesher will be used in this study, which produces a high quality grid for complex mesh-generating problems and it also presents high orthogonality to the mean free stream flow. The trimmer is used to specify mesh properties on the specific volumetric controls, which makes up final mesh. As shown in Figure 4-5, Figure 4-6 and Figure 4-7 the refined mesh around the free surface, tank bottom, each bank sides, around hull and in the wake region is created to capture the complex flow features. After the volumetric meshing type is selected, Star-CCM+ provides the prism layer mesher to resolve boundary layer near the walls and to obtain correct wall shear stress on the hull. The prism layers are created with a total thickness corresponding to the estimated boundary layer thickness. The number of cell layers within the prism mesh, and the height of the prism cell layer next to wall are specified to obtain a proper value of y^+. To avoid numerical difficulty for shallow water cases, y^+ is larger than 45 so as to

use the wall function on the tank bottom and the close side tank wall. y^+ is set to be smaller than 1 at the hull surface to obtain a more correct flow field simulation near the ship.

In the present study, an overset mesh is used to facilitate the motions of the ship model. When using the overset mesh method, the domain is divided into a stationary background region and a moving overset region.

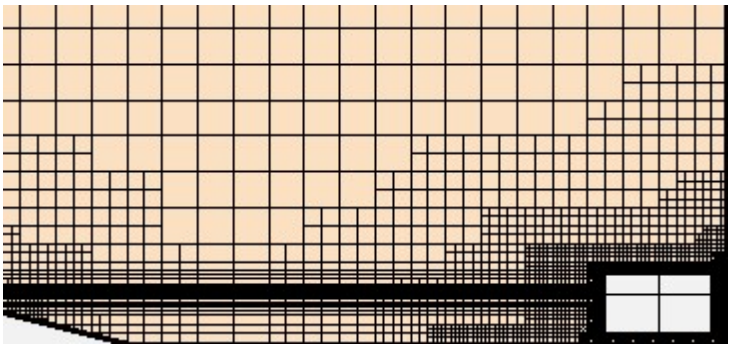

Figure 4-5 Cross sectional front view of the volume mesh (x=0)

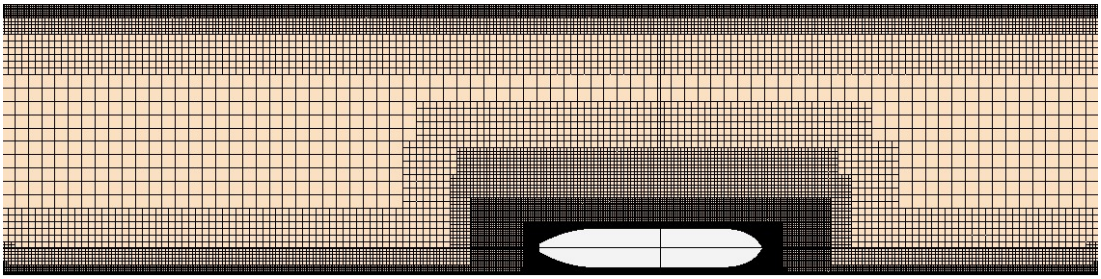

Figure 4-6 Cross sectional top view of the volume mesh (z=0)

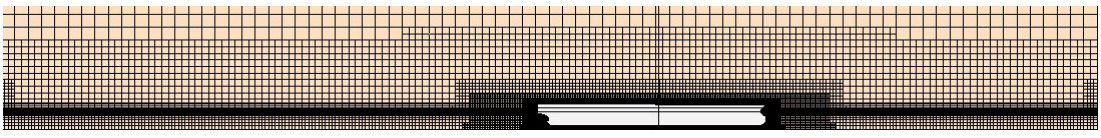

Figure 4-7 Cross sectional side view of the volume mesh (y=0)

4.6 Physic models

In this section, various physic models are chosen and described. The physics continuum manager in Star-CCM+ provides the options of physical model. Therefore, the flow solver, material models, steady or transient time model, a turbulence model should be selected.

The time model selected in this study is an implicit unsteady model, which is most suitable for the present problem. The Volume of Fluid (VOF) method is used to simulate the free surface with a flat wave. The VOF method is defined as a simple multiphase model that is appropriate for simulating the flows of several immiscible fluids on numerical grids. It enables the solution of the interface between the phase of the air and the water in CD-Adapco (2017), since it provides high efficiency. This model is also proper for simulating the flows where each phase forms a large structure. The turbulence model chosen in this study is the $k-\varepsilon$ turbulence model, as described in Chapter 3.3. Two-layer all y^+ wall treatment is automatically selected when the $k-\varepsilon$ turbulence model is selected.

In this study, the Dynamic Fluid Body Interaction (DFBI) module is used to simulate the dynamic behaviour of the ship. It enables the vessel to be free in sinkage and trim. The DFBI module is suitable when the hydrodynamic forces and moments acting on the hull is required to be calculated. The governing equations of rigid body motion is needed to solve for the RANS solver.

The time step is determined by using the Courant number (CFL), which is the ratio of the physical time step (Δt) to the mesh convection time scale, relates the mesh dimension Δx to the mesh flow speed *U* as given below:

$$\mathrm{CFL} = \frac{U\Delta t}{\Delta x} \tag{4.1}$$

To achieve time-accurate simulations, an average value of 1 is required for CFL in all cell. It means that the flow moves by about one cell size at each time step. The average Courant number requires to be less than 0.5 for the second-order scheme for time integration

For all the simulations, the implicit unsteady model is used in this study. The time step is often set by the flow properties, rather than the Courant number in implicit unsteady computation. The time-step size is determined by $\Delta t = 0.005 - 0.01 L/v$ (where L is the length between perpendiculars and v is the ship speed) for resistance simulation in calm water, based on the related guidelines of ITTC (2011). For this study, to determine the optimal time-step resolution, the results from the time-step convergence study conducted resulted in employing the much smaller time step $\Delta t = 0.004 L/v$ ($\Delta t = 0.05 s$).

5 Simulation results

5.1 Remarks

This chapter describes the numerical results for the simulations, including the results of the grid convergence test, hydrodynamic forces or moments, sinkage, trim, wave elevation and pressure distribution. The numerical results will be validated against the experimental results carried out by Hoydonck, et al. (2015).

5.2 Verification study

Prior to the numerical computations, a verification study is always suggested to quantify the numerical and modelling errors in the computations. This will be accomplished by the grid convergence tests.

In the numerical method the hydrodynamic problem is formulated by mathematical equations which generally has to be discretized in space and time. From a theoretical point of view, the discretization error should approach zero when the number of grid points tends to infinity. However, since the number of grid points is limited there are always discretization errors. To estimate this error and to obtain more reliable results from a numerical point of view, the verification of the computation is essential, and a so-called convergence study is always required.

The preliminary grid convergence computations are carried out for the cases similar with Case 1. To simplify the computation, sinkage and trim are assumed to be negligible. Computational settings (coordinate system, domain, grid generation, boundary conditions, etc.) in the grid convergence study are consistent with the descriptions in Chapter 4.

The estimation of numerical errors and uncertainties followed the procedure proposed by Eça, et al. (2010a) and Eça, et al. (2010b). Five systematically refined grids were created and a uniform grid refinement ratio $r = \sqrt[3]{2}$ was used to create the

systematically similar grids. The number of cells and the size of cell were given in Table 5-1, from the finest grid to the coarsest grid.

Table 5-1 Grid sizes in grid convergence study for case 1

No.	h_i/h_1 $(i = 1, 2, \dots, 5)$	Number of cells
Grid 1	1.0	7,472,866
Grid 2	1.260	4,511,952
Grid 3	1.587	2,633,647
Grid 4	2.0	1,857,790
Grid 5	2.520	1,279,866

The grid convergence study was made for the non-dimensional longitudinal and sway force, yaw moment coefficients, which are defined as follows:

$$\mathrm{X}' = \frac{X}{0.5\rho U_0^2 L_{pp} T}$$

$$\mathrm{Y}' = \frac{Y}{0.5\rho U_0^2 L_{pp} T} \tag{5.1}$$

$$\mathrm{N}' = \frac{N}{0.5\rho U_0^2 L_{pp}^2 T}$$

Figure 5-1 presents the results of the convergence study. From the results of the grid convergence study, it can be concluded that it is very difficult to obtain grid convergence in ship-bank interaction problem. The hydrodynamic quantities predicted by using the finest grids are still fluctuating or converge slowly. The finest grid discretization (i.e., approximately, 7.5 million grid points) does not help to obtain a convergent results. This conclusion confirms the observations by Zou and Larsson (2013), in which large uncertainties were found in ship-bank interaction problem. The computing expenses are always considered in the simulations. The computational time and the numerical accuracy have to be balanced. That is why it suggests that Grid 3 can be adopted in the rest of the systematic computations of bank effects in this study.

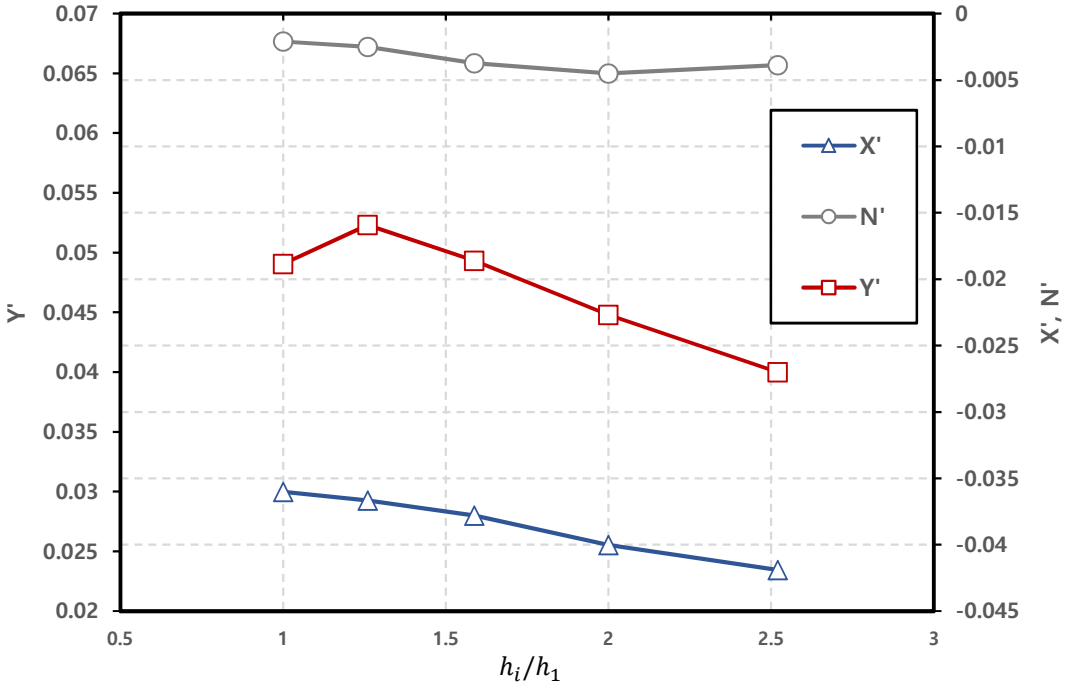

Figure 5-1 Grid convergence of X', Y', N'

5.3 Validation study

5.3.1 Comparison of forces and moments

The results of the longitudinal, lateral forces and yaw moments (*X, Y, N*) at different *d/B* and *h/T* ratios are presented in Figure 5-2 and Figure 5-3. The experimental results, as well some numerical results, are also included in these figures. Figure 5-2 shows the results for *X, Y* forces and *N* moments at a specific water depth, *h/T* = 1.35, against the distance to the bank. Figure 5-3 shows the results at a specific distance to the bank, *d/B* = 1.26, against the water depth. EFD which represents the model test results and the results from ISIS-CFD and ReFRESCO are provided by Hoydonck, et al. (2015). ISIS-CFD represents the results obtained by an incompressible, Reynolds-averaged Navier-Stokes (URANS) solver by using a first-order time discretization; ReFRESCO represents the results obtained by URANS solver by using a second-order time discretization; ReFRESCO is a viscous-flow CFD code that solves multiphase

(unsteady) incompressible flows with the RANS equations; ROPES is a 3D potential flow program by using rigid wall condition on free-surface. The results from RPOES are referred to Vaz et al (2009); SHIPFLOW is a steady state CFD software which contains a RANS solver. The results from SHIPFLOW are referred to Zou and Larsson (2013).

As can be seen, the present results from STAR-CCM+ agree well with the experimental results. Comparing with the results from other programmes, the tendencies of hydrodynamic forces and moments predicted in the present study are captured well.

It can be concluded from Figure 5-2 that as ratio of *d/B* becomes smaller, the longitudinal and lateral forces increase rapidly, while a few difference was noticed in the yaw moments. However, the results of sway force and yaw moment predicted by ROPES is incorrect compared to the results of this study and other CFD results. That is because ROPES neglects the free-surface effects. It can also be seen from Figure 5-3 that the longitudinal forces and yaw moments increase rapidly as ratio of *h/T* becomes smaller. Overall, the results of this study represent similar results compared to other CFD results.

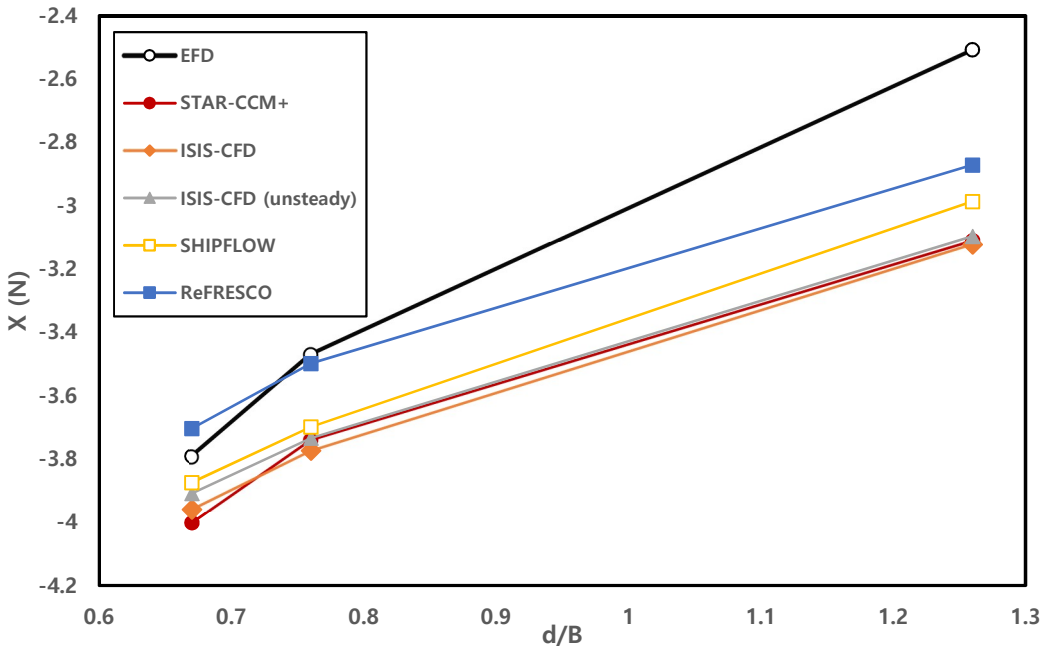
-2.4
-2.6
-2.8
-3
-3.2
-3.4
-3.6
-3.8
-4
-4.2
X (N)
0.6
0.7
0.8
0.9
1
1.1
1.2
1.3
d/B
EFD
STAR-CCM+
ISIS-CFD
ISIS-CFD (unsteady)
SHIPFLOW
ReFRESCO

(a)

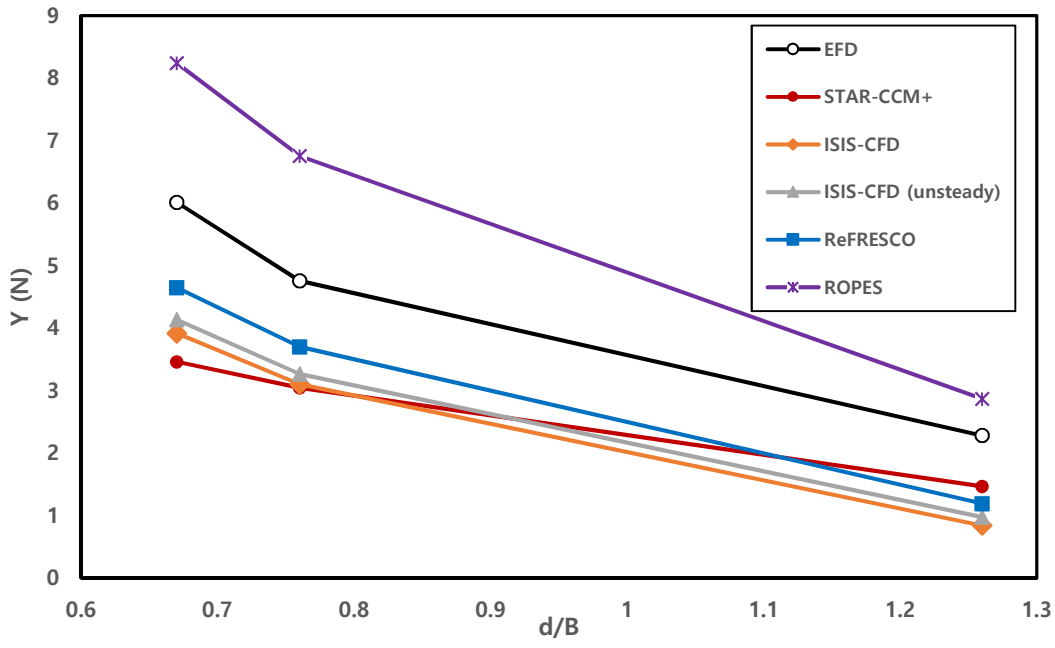
9
8
7
6
5
4
3
2
1
0
Y (N)
0.6
0.7
0.8
0.9
1
1.1
1.2
1.3
d/B
EFD
STAR-CCM+
ISIS-CFD
ISIS-CFD (unsteady)
ReFRESCO
ROPES

(b)

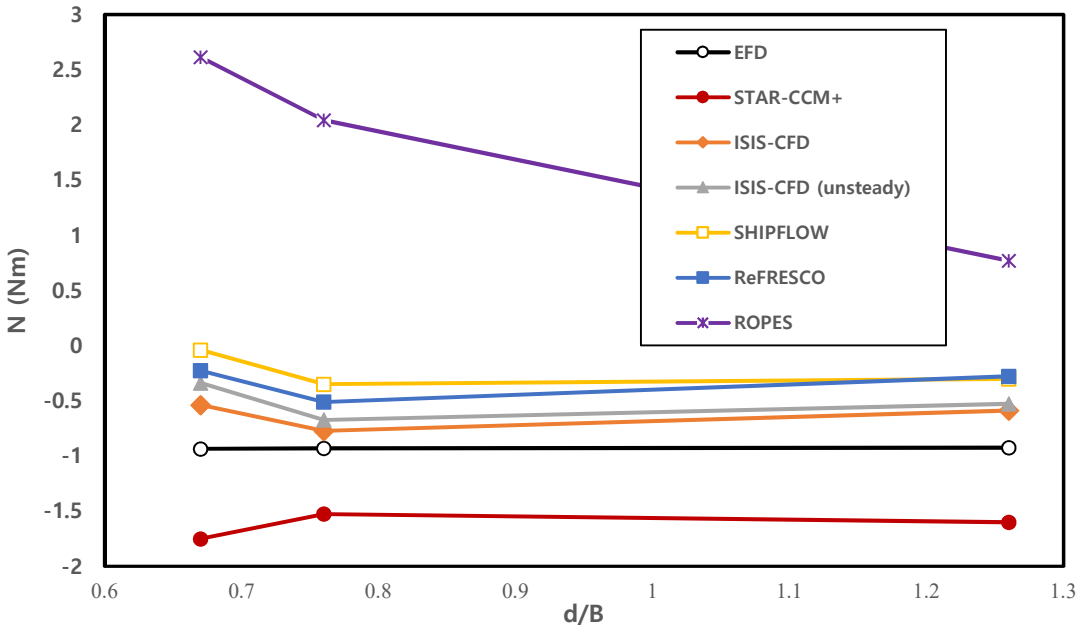

(c)

Figure 5-2 Comparison of forces and moments at different ratio of *d/B* from different program (a) Longitudinal forces (b) Lateral forces (c) yawing moments

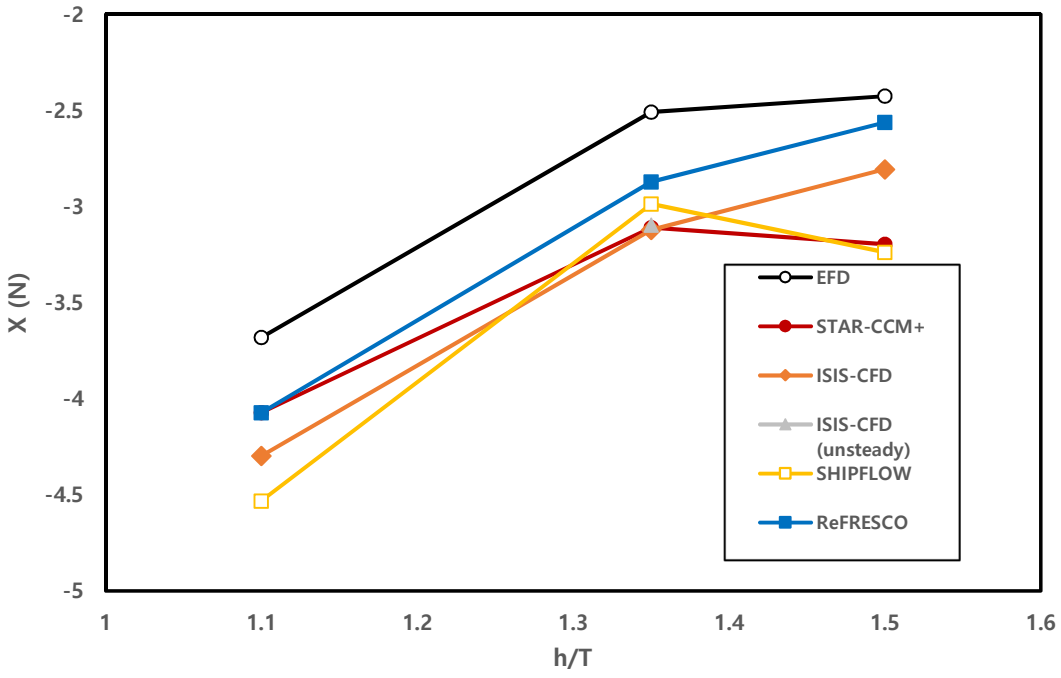

(a)

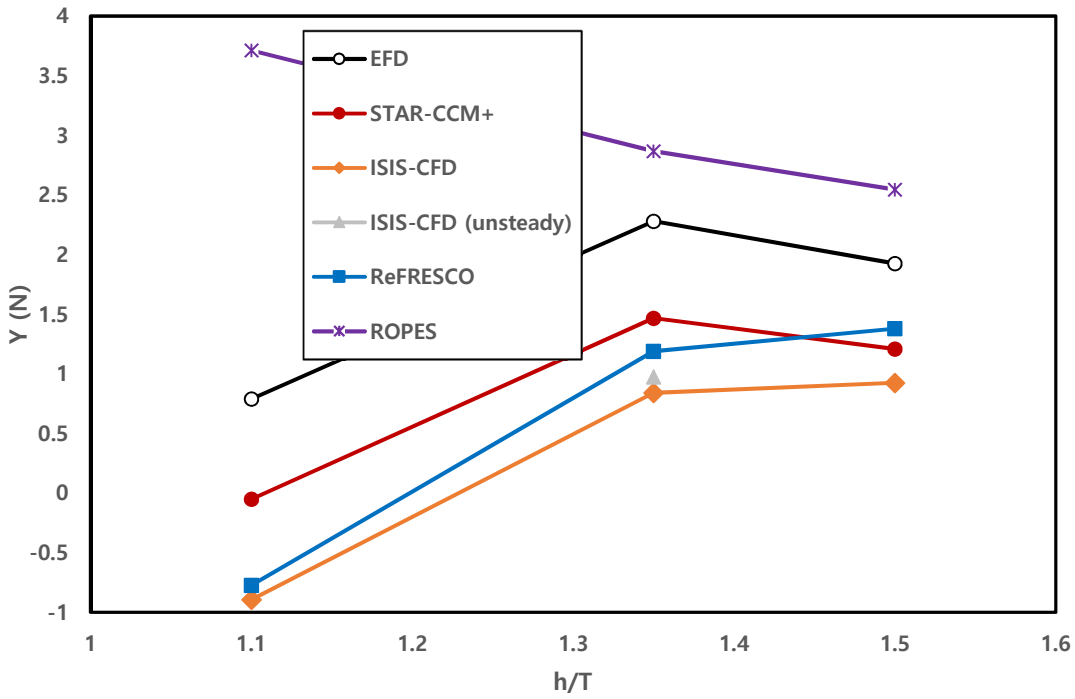

(b)

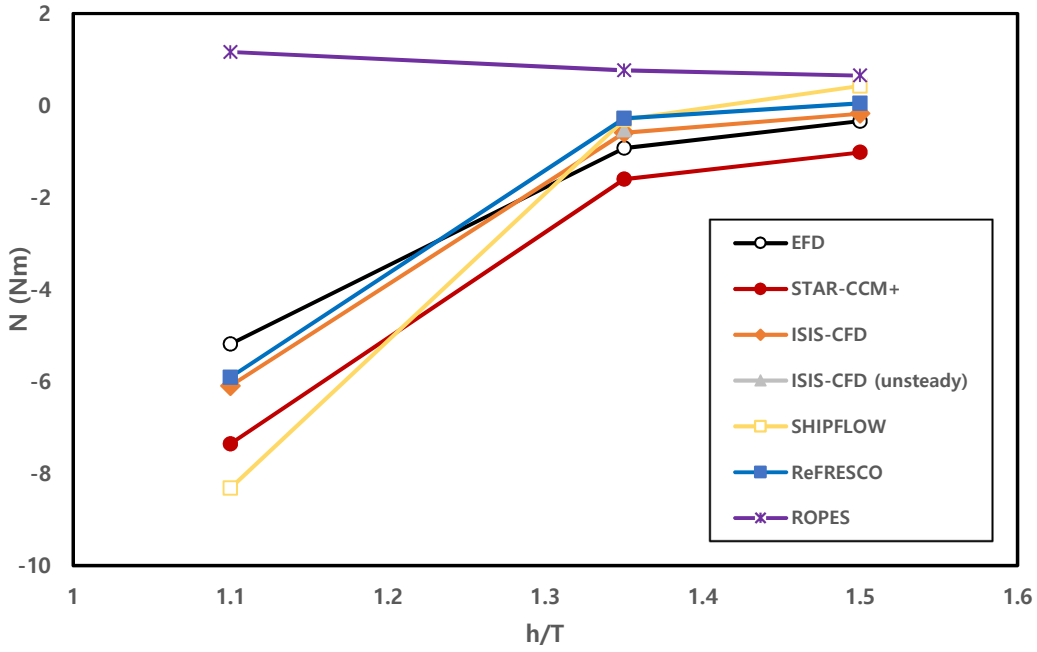

(c)

Figure 5-3 Comparison of forces and moments at different ratio of *h/T* from different program (a) Longitudinal forces (b) Lateral forces (c) yawing moments

5.3.2 Comparison of sinkage and trim

In this section, the results with various water depths, ship-bank distances and speeds are presented. The sinkage is positive downwards and trim is positive bow-up. The computed results of the sinkage and trim from the RANS method are plotted in Figure 5-4 and Figure 5-5, accompanied by the experimental data. Figure 5-4 shows the sinkage and trim results versus the ship-bank distance at the same water depth ratio h/T=1.35, while Figure 5-5 shows the results at a specific distance to the bank, d/B = 1.26, against the water depth.

The sinkage increases as the water depth decreases at the same forward speed. The sinkage is larger when the ship is getting closer to the bank. The computed sinkage and trim qualitatively follow the same trend as the measurements with slight under-prediction. The difference between experimental and numerical results of the sinkage is due to the fact that the sinkage are too small, which is difficult to capture precisely.

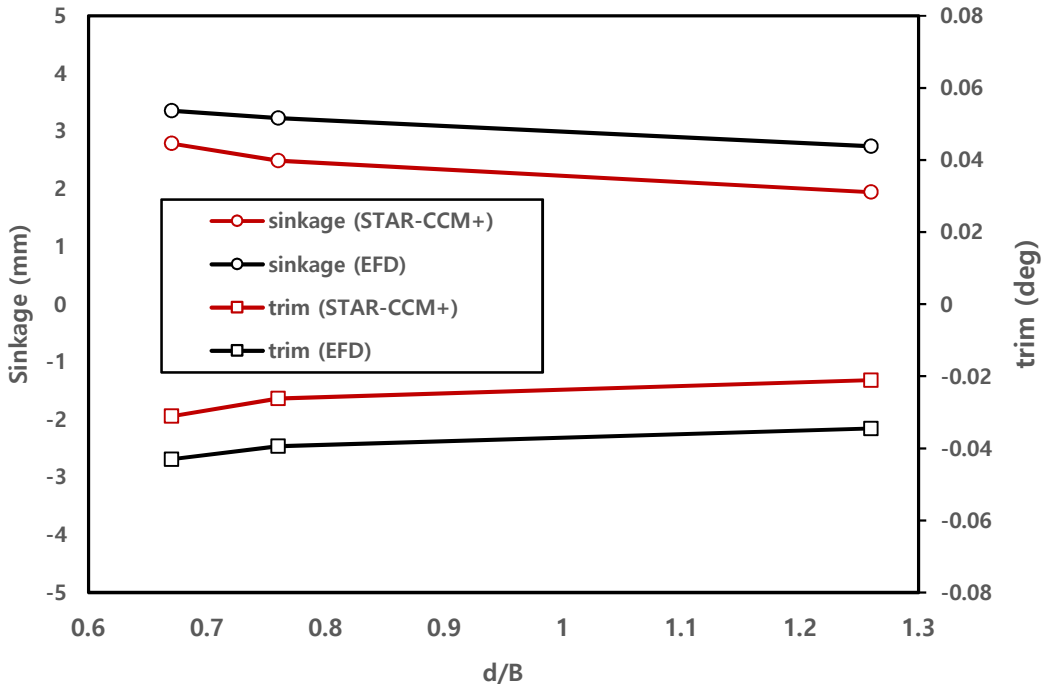

Figure 5-4 Comparison of sinkage and trim at different ratios of d/B

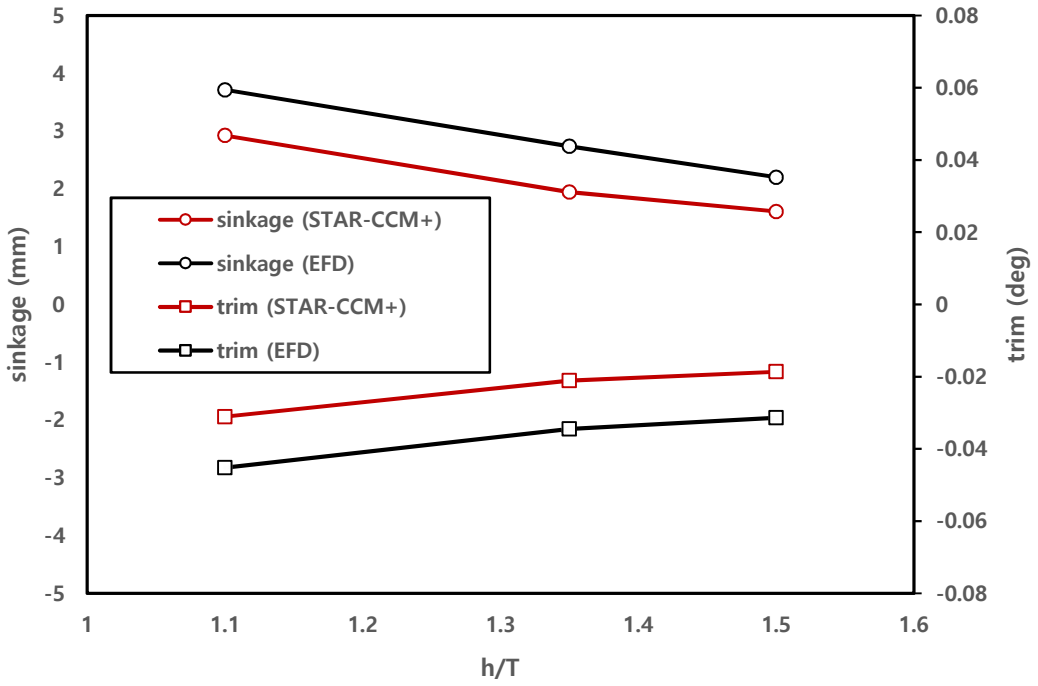

Figure 5-5 Comparison of sinkage and trim at different ratios of *h/T*

5.3.3 Comparison of wave elevation

For the STAR-CCM+ computations, the results of the water surface elevation are obtained along a line parallel to the quay, $0.02m$ from the bank. The longitudinal coordinate is made dimensionless using the characteristic ship length L_{pp} and an offset is applied to set the origin at the mid-ship location. After a conversion to millimetre, the results, as shown in Figures 5-6 to 5-10, are obtained. It can be observed that the agreement between the present predictions and the experimental measurements is generally satisfactory around the ship, but there are some disagreements around the inlet and outlet boundary regions.

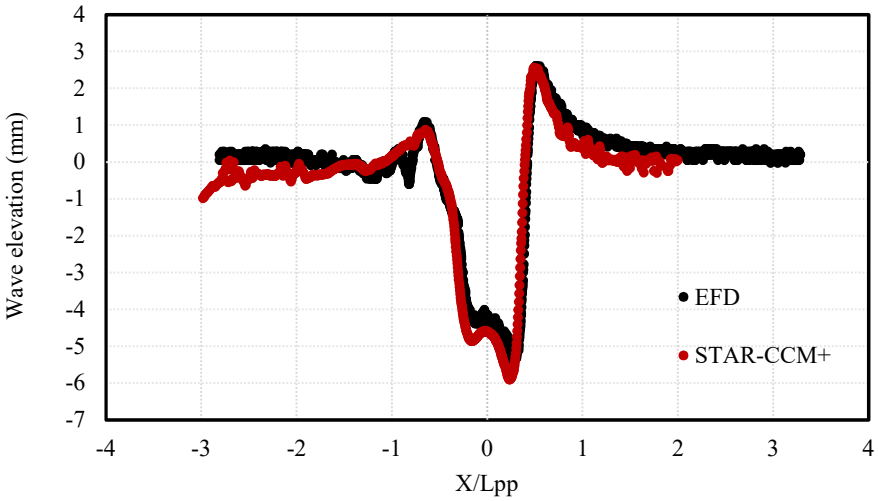

Figure 5-6 Results of wave elevation (case 1)

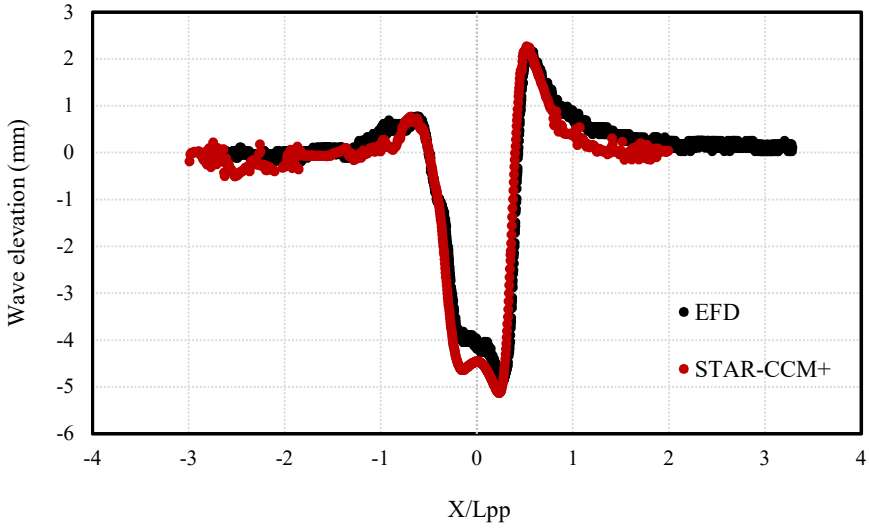

Figure 5-7 Results of wave elevation (case 2)

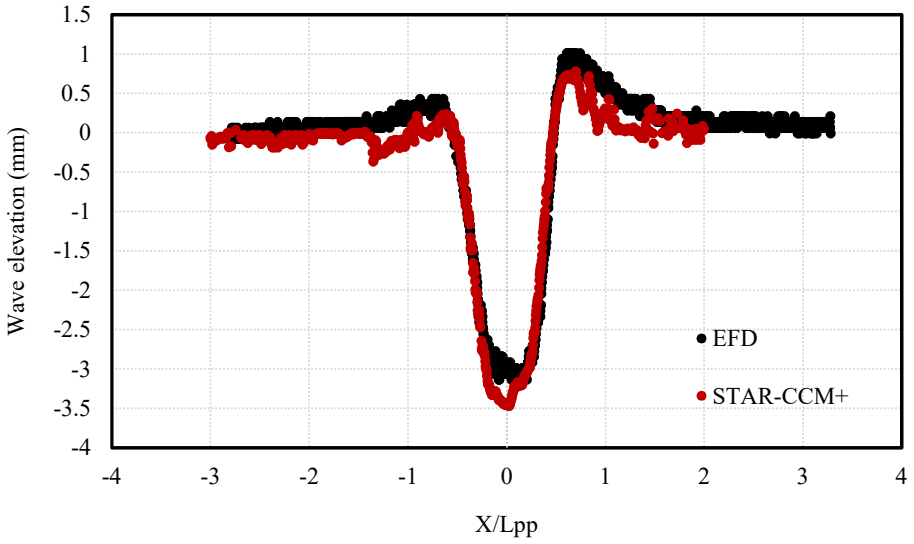

Figure 5-8 Results of wave elevation (case 3)

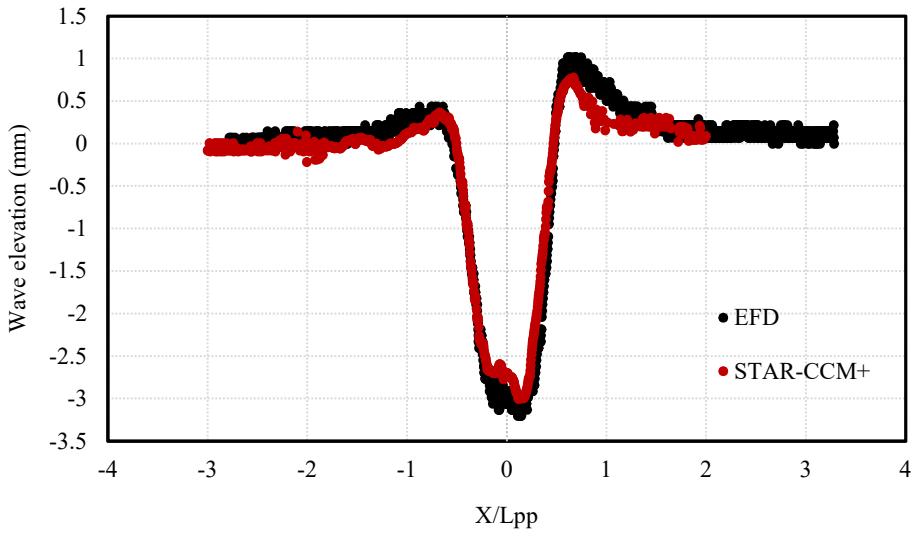

Figure 5-9 Results of wave elevation (case 4)

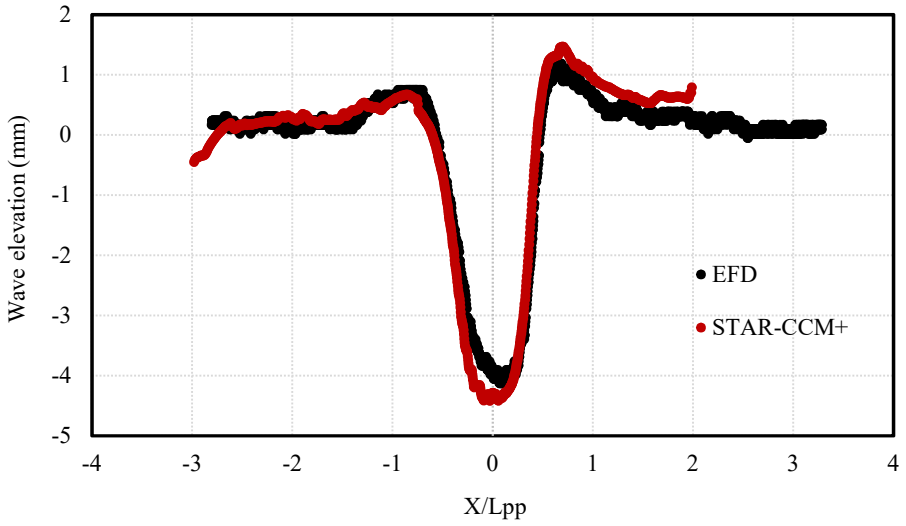

Figure 5-10 Results of wave elevation (case 5)

5.4 Pressure distribution

In this section, the dynamic pressure distribution over the ship hull, and the bottom and bank of the channel are discussed. As shown in Figure 5-11, when the ship-to-bank distance decreases, a lower pressure distributed over the starboard side of the ship hull can be observed. It results in an increase of suction force towards the bank. The difference between the pressure distribution in the starboard and portside is not obvious when the ship-to-bank distance is large, for example d/B =1.25, as shown in Figure 5-11 (c). As the ship-to-bank distance decreases, the pressure difference becomes evident, as shown in Figure 5-11 (a) and (b). In general, lower pressures region around the ship hull is observed when the water depth decreases, resulting from the blockage effect. This can be easily seen in Figure 5-12, which also shows a very large pressure distributed over the ship bow.

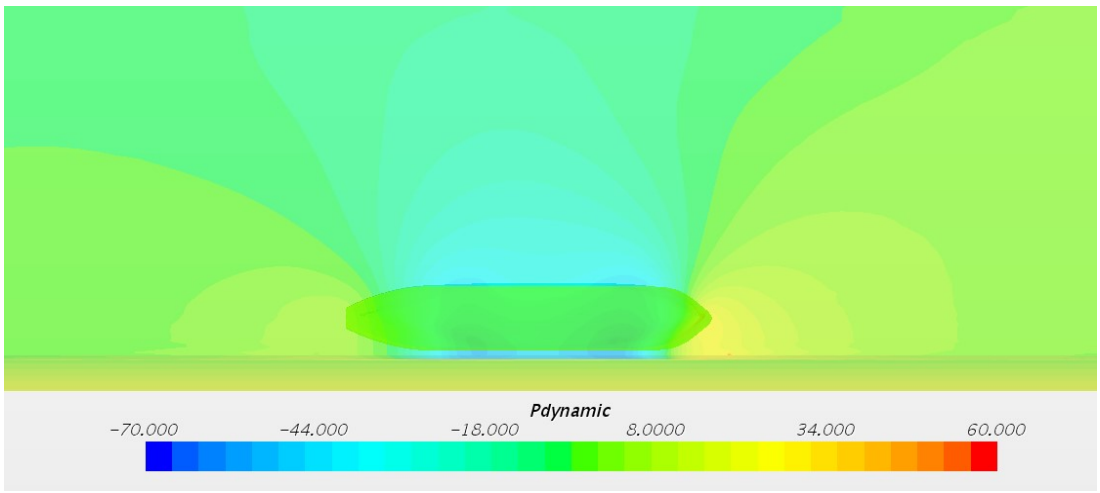

(a) d/B = 0.67

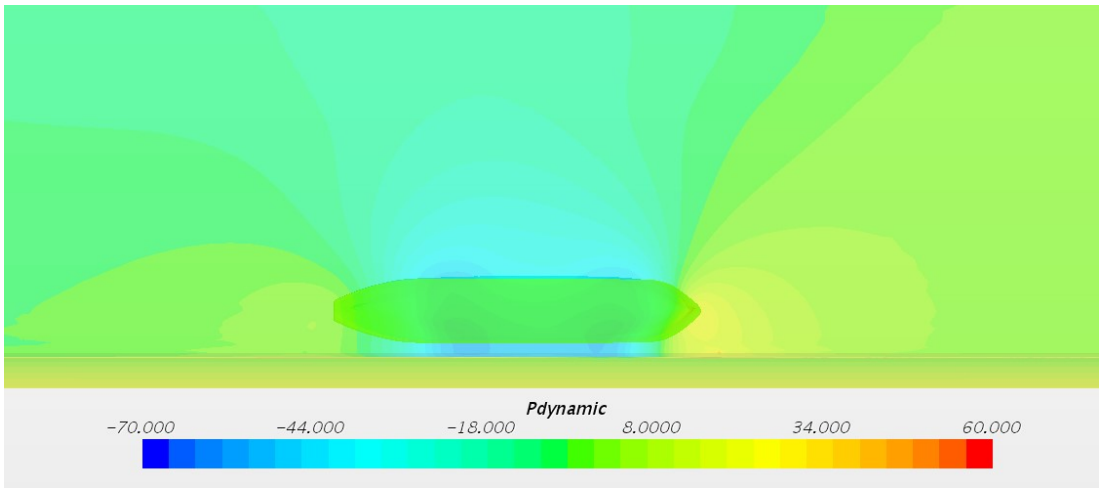

(b) d/B = 0.76

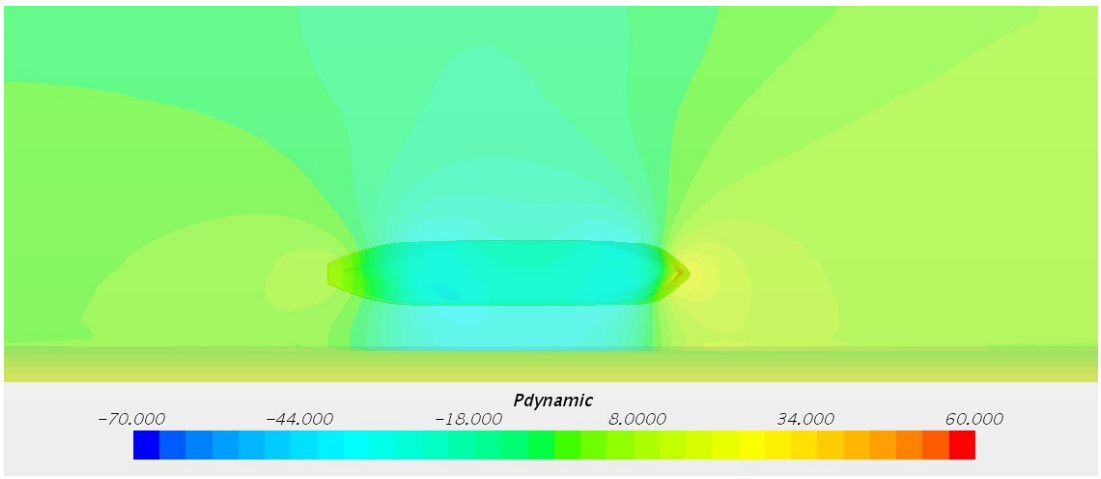

(c) d/B = 1.26

Figure 5-11 Dynamic pressure at different d/B

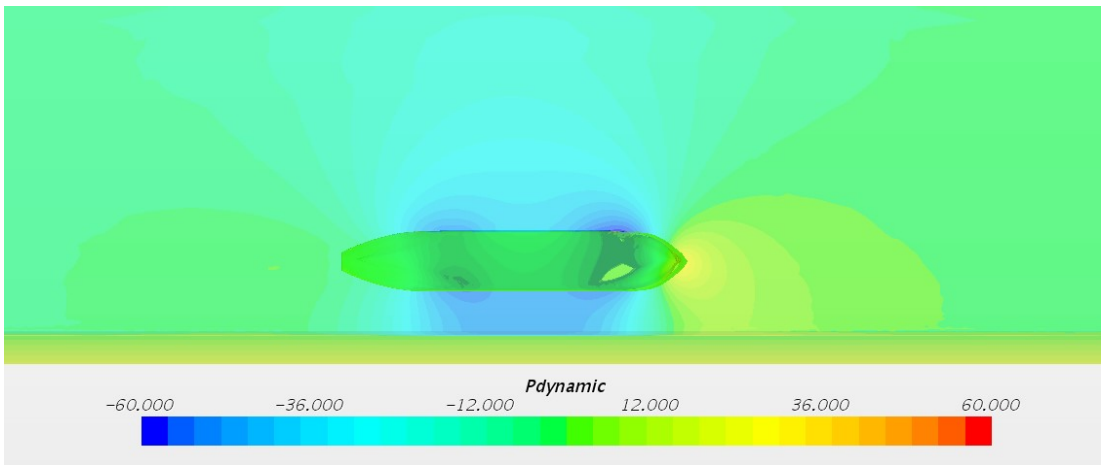

(a) h/T = 1.1

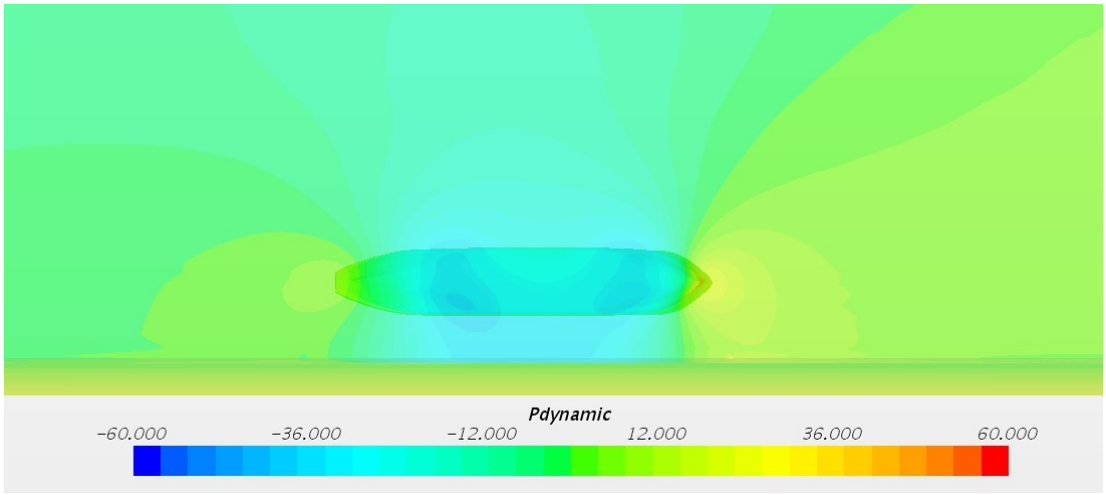

(b) h/T = 1.35

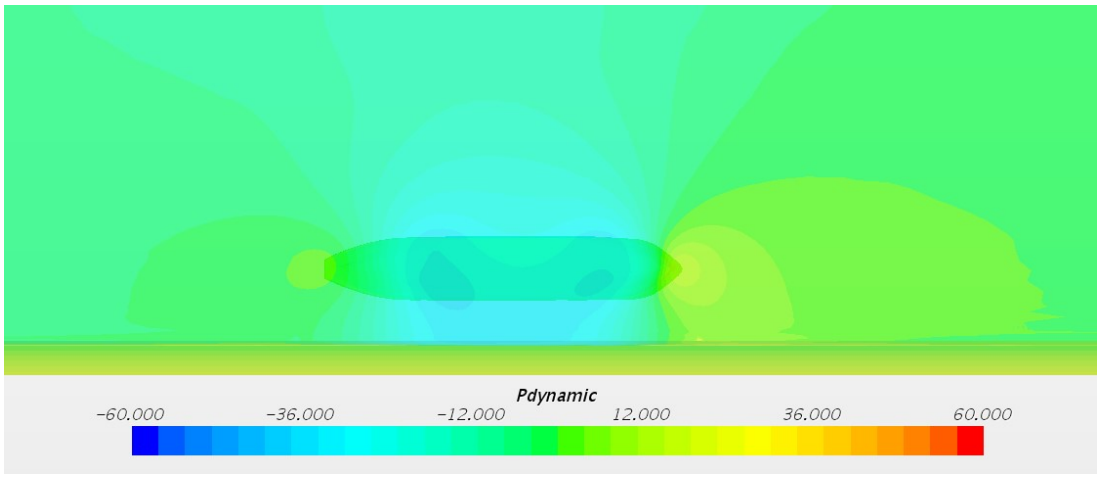

(c) h/T = 1.5

Figure 5-12 Dynamic pressure at different h/T

5.5 Forces and moments at different ship speeds

It is important to know the effect of advancing speed when a ship is advancing in confined waterways. The results of the longitudinal, lateral forces and the yaw moments (*X, Y, N*) at different ship speeds are presented in Figure 5-13. The water depth is fixed at $h/T = 1.35$ and the ship-to-bank distance is fixed at $d/B = 0.67$.

It can be concluded from Figure 5-13 that as the ship speed becomes larger, the longitudinal and lateral forces increase rapidly, while a few difference can be observed in the yaw moments.

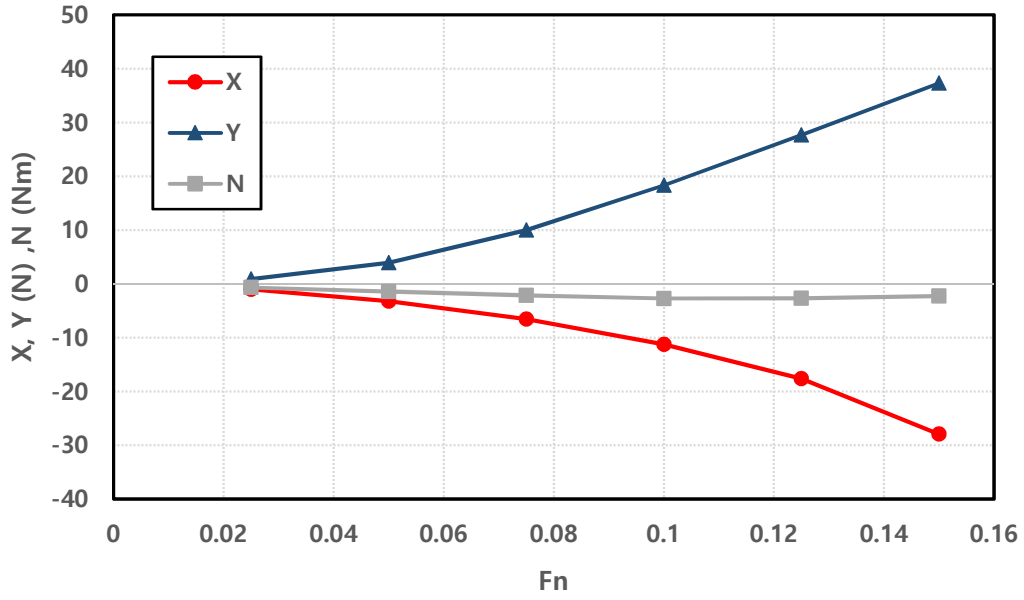

Figure 5-13 Forces and moments at different ship speeds

6 Conclusion

Predicting ship hydrodynamics in confined waterways is a challenging task due to the importance and complexity of the hydrodynamic interactions. Due to the strong interaction between ships and the bank/bottom of the waterways, it is very difficult to model the physical problem by numerical tools. In the present study, the hydrodynamic performance of a ship advancing in confined waterways is investigated by using a numerical tool, STAR-CCM+. Validations are conducted by comparing the numerical results with experimental measurements.

Firstly, a grid convergence study was performed for Case 1 to obtain the numerical uncertainty in the computations by varying grid densities, following the procedure by Eça, et al. (2010a) and Eça, et al. (2010b). The results of the study showed the difficulty in obtaining converged results in ship-bank interaction problem and this conclusion was also indicated in the study by Zou and Larsson (2013).

Then, the results of the sinkage, trim, as well as the hydrodynamic forces and moments on the ship advancing in various water depths and ship-to-bank distances were investigated. The numerical results were compared to the experimental measurements, as well as published CFD results by Hoydonck, et al. (2015). The general agreement between the present CFD results and the experimental measurements is satisfactory.

Furthermore, the dynamic pressure distributed over the ship hull, and the bottom/bank was calculated. It was shown that when the ship-to-bank distance and the water depth decreased, a lower pressure distributed over the starboard sides of the ship was observed.

Finally, the hydrodynamic forces and moments on a ship advancing at different speeds were investigated. It was clearly shown that the hydrodynamic forces became larger as the speed increased. However, the yaw moment was not influenced by the ship speed.

The overall conclusion of the study is that it is feasible to predict the bank effects by using CFD method. However, the effect of the propeller is not assessed in the present study. Therefore, it would be of interest to investigate the effect of the propulsion in the tank equipped with the surface-piercing bank and the vertical quay wall in the future study.

Reference

Alderf, N., Lefrancois, E., Sergent, P. & Debaillon, P., 2009. Dynamic ship response integration for numerical prediction of squat in highly restricted waterways.. *International Journal for Numerical Methods in Fluids,* 65(7), pp. 743-763.

Beck, R. F., 1977. Forces and moments on a ship moving in a shallow channel. *Journal of Ship Research,* 21(2), pp. 107-119.

Beck, R. F., Newman, J. N. & Tuck, E. O., 1975. Hydrodynamic forces on ships in dredged channels. *Journal of Ship Research,* 19(3), pp. 166-171.

CD-Adpaco, 2017. *User guide STAR-CCM+ (Version 12.06.011).*

Chetvertakov, A. M., Lebedeva, M. P., Nikushchenko, D. V. & Maritime, K., 2011. *Numerical investigation of bank influence on a ship motion.* Trondheim, Norway, 2nd International Conference on Ship Manoeuvring in Shallow and Confined Water: Ship to Ship Interaction.

Ch'ng, P. W., Doctors, L. J. & Renilson, M. R., 1993. A method of calculating the ship-bank interaction forces and moments in restricted water. *International Shipbuilding Progress,* 40(421), pp. 7-23.

Dand, I. W., 1982. *On ship-bank interaction.* London, UK, Transactions of the Royal Institution of Naval Architects.

Date, J. C. & Turnock, S. R., 1999. *A study into the techniques needed to accurately predict skin friction using RANS solvers with validation against Froude's historical flat plate experimental data.* 14 ed. Southampton, UK: University of Southampton.

Demuren, A., 1985. False Diffusion in Three-Dimensional Flow Calculation. *Computers & Fluids,* 13(4), pp. 411-419.

Eça, L., Vaz, G. & Hoekstra, M., 2010a. *A verification and validation exercise for the flow over a backward facing step.* Lisbon, Portugal, V European Conference on Computational Fluid Dynamics, ECCOMAS CFD 2010.

Eça, L., Vaz, G. & Hoekstra, M., 2010b. *Code verification, solution verification and validation in RANS solvers.* Shanghai, China, ASME 29th internatioinal OMAE 2010.

Fuehrer, M., 1978. *The Results of Systematic Investigations into Lateral Forces for Determining the Effects of Hydraulic Asymmetry and Eccentricity on the Navigation of Seagoing Ships in Canals.* Delft, Netherlands, Symposium Aspects of Navigability of Constraint Waterways.

Fuehrer, M. & Römisch, K., 1983. The effects of hydrodynamic forces on ships navigating through canal - A contribution to an estimation of the manoeuvrability of ships in a restricted channel. *Bulletin of the Permanant International Association of Navigation Congress,* 57(43), pp. 10-20.

Gates, E. T. & Herbich, J. B., 1977. Mathematical models for the design, Operation and economic analysis of deep-draft navigation channels. *International Navigation Congress,* pp. 175-182.

Gourlay, T., 2008. Slender-body methods for predicting ship squat. *Ocean Engineering,* 35(2), pp. 191-200.

Gronarz, A., 2009. *Investigation of the influence of a vertical wall on a ship moving with drift angle.* Antwerp, Belgium, International Conference on Ship Manoeuvring in Shallow and Confined Water: Bank Effects.

Hoydonck, W. V. et al., 2015. *Bank effects for KVLCC2.* Rhode Island, USA, World Maritime Technology Conference.

ITTC, 2011. *ITTC Recommended procedure and guideline - Practical guidelines for ship CFD application.*

ITTC, 2017. *ITTC Recommended procedure and guideline - Guidline on Use of RANS Tools for Manoeuvring Prediction.*

Jachowski, J., 2008. Assessment of ship squat in shallow water using CFD. *Elsevier Archives of Civil and Mechanical Engineering,* 8(1), pp. 27-36.

Kobylinski, L., 2014. Bank effect and operation of inland waterways vessels. *Scientific Journals,* p. 51.

Kumar, M. & Anantha Subramanian, V., 2007. A numerical and experimental study on tank wall influences in drag estimation. *Ocean Engineering,* 34(1), pp. 192-205.

Lataire, E., Vantorre, M. & Eloot, K., 2009. *Systematic model tests on ship-bank interaction effects.* Antwerp, International conference on ship manoeuvring in shallow and confined water: bank effects.

Li, D. Q., Leer-Andersen, M., Ottosson, P. & Trägårdh, P., 2001. *Experimental investigation of bank effects under extreme conditions.* Shanghai, China, Practical design of ships and other floating structure.

Maimum, A. et al., 2013. A mathematical model on manoeuvrability of a LNG tanker in vicinity of bank in restrected water. *Safety Science,* Volume 53, pp. 34-44.

Miao, Q. M., Xia, J. Z. & Chwang, A. T., 2003. *Numerical study of bank effects on a ship travelling in a channel.* Busan, 8th international conference on numerical ship hydrodynamics.

Newman, J. N., 1969. Lateral motion of a slender body between two parallel walls. *Journal of Fluid Mechanics,* 39(01), pp. 97-115.

Norrbin, N. H., 1974. *Bank effects on a ship moving through a short dredged channel.* Cambridge, 10th Symposium on naval hydrodynamics.

Norrbin, N. H., 1985. Bank clearance and optimal section shape for ship canals. *26th International Navigation Congress,* pp. 167-178.

Peric, F. M. & Joel, H., 1997. *Computational Methods for Fluid Dynamics.* second edition ed. s.l.:Springer.

Quérard, A., Temarel, P. & Tumock, S., 2008. Influence of viscous effects on the hydrodynamics of ship-like sections undergoing symmetric and anti-sysmmetric motions, using RANS. *ASME 2008 27th International Conference on Offshore Mechanics and Arctic Engineering,* 692(5), p. 683.

Römisch, K., 1978. *Contribution to a determination of the required canal width.* Delft, Netherlands, Symposium Aspects of Navigability of Contraint Waterways.

Tezdogan, T., Incecik, A. & Turan, O., 2016. A numerical investigation of the squat and resistance of ships advancing through a canal using CFD. *Journal of Marine Science and Technology,* 21(1), pp. 86-101.

Tuck, E. O., 1966. Shallow-water flows past slender bodies. *Journal of Fluid Mechanics,* 26(1), pp. 81-95.

Vantorre, M., 2002. *Modelling of ship-bank interaction forces.* Duisburg, The ship interaction with the waterway.

Vantorre, M., Delefortrie, G., Eloot, K. & Laforce, E., 2003. *Experimental investigation of ship-bank interaction forces.* Kanazawa, Japan, International Conference on Marine Simulation and Ship Manoeuvrability, MARSIM 2003.

Vaz, G., Jaouen, F. & Hoekstra, M., 2009. *Free surface viscous flow computations. Validation of URANS code FRESCO.* Honolulu, Hawaii, 28th International Conference on Ocean, Offshore and Arctic Engineering.

Versteeg, H. K. & Malalasekera, W., 2007. *An Introduction to Computational Fluid Dynamics: The Finite Volume Method.* second edition ed. England: Harlow: Pearson Education Limited.

Wang, H., Zou, Z., Xie, Y. & Kong, W., 2010. *Numerical study of viscous hydrodynamic forces on a ship navigating near bank in shallow water.*. Beijing, The twentieth international offshore and polar engineering conference.

White, F., 2006. *Viscous Fluid Flow.* 3 ed. s.l.:McGraw-Hill Higher Education.

Wilcox, D. C., 2006. *Turbulence modelling for CFD.* 3rd Edition ed. USA: DCW Industries Incoporated.

Yasukawa, H., 1991. Effects of unsymmetric flow on a ship traveling in a channel. *Journal of Ship Mechanics,* 8(3), pp. 1-12.

Zou, L. & Larsson, L., 2013. Confined water effects on the viscous flow around a tanker with propeller and rudder. *International Shipbuilding Progress,* 60(1-4), pp. 101-125.

Zou, L., Larsson, L., Delefortrie, G. & Lataire, E., 2011. *CFD prediction and validation of ship-bank interaction in a canal.* Trondheim, 2nd International

Conference on Ship Manoeuvring in Shallow and Confined Water: Ship to Ship Interaction.